AD-A094 290 COLORADO UNIV AT BOULDER DEPT OF MECHANICAL ENGINEERING F/G 10/2
EFFECTIVE TECHNIQUES FOR AUGMENTING HEAT TRANSFER: AN APPLICATI--ETC(U)
DEC 80 A BEJAN N00014-79-C-0006
UNCLASSIFIED CUMER-80-9 NL

1 OF 1
AD A094290

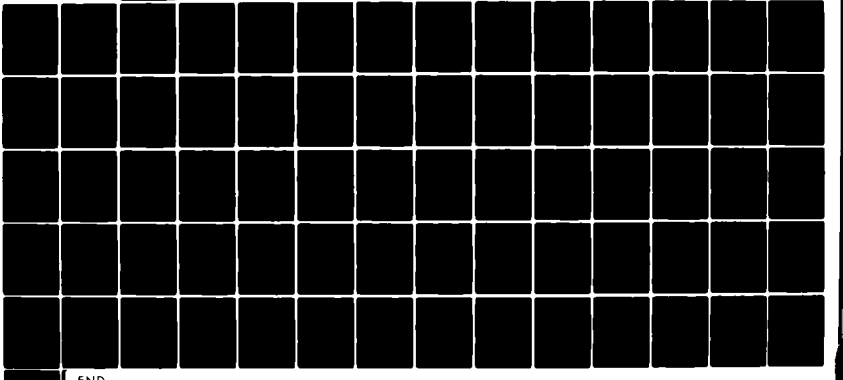

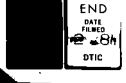

LEVEL II

12

UNIVERSITY OF COLORADO

AD A094290

DEPARTMENT OF
MECHANICAL ENGINEERING

College of Engineering
Boulder, Colorado

(12)

(9) F... 1 ... 78-3/ ... 1,

EFFECTIVE TECHNIQUES FOR AUGMENTING HEAT TRANSFER: AN APPLICATION OF ENTROPY GENERATION MINIMIZATION PRINCIPLES

(10) Adrian Bejan

(14) Report CUMER-80-9 (11) December 1980

(12) 87

(15) N...14-...-...-...

(16) N...-...-...

(17) ...

40...

Unclassified
SECURITY CLASSIFICATION OF THIS PAGE (When Data Entered)

REPORT DOCUMENTATION PAGE	READ INSTRUCTIONS BEFORE COMPLETING FORM
1. REPORT NUMBER: CUMER-80-9	2. GOVT ACCESSION NO.: AD-A094290
	3. RECIPIENT'S CATALOG NUMBER:
4. TITLE (and Subtitle): EFFECTIVE TECHNIQUES FOR AUGMENTING HEAT TRANSFER	5. TYPE OF REPORT & PERIOD COVERED: Final, Oct. 1, 1978-Sept. 30, 1980
	6. PERFORMING ORG. REPORT NUMBER:
7. AUTHOR(s): Adrian Bejan	8. CONTRACT OR GRANT NUMBER(s): N00014-79-C-0006
9. PERFORMING ORGANIZATION NAME AND ADDRESS: Department of Mechanical Engineering, University of Colorado, Boulder, Colorado 80309	10. PROGRAM ELEMENT, PROJECT, TASK AREA & WORK UNIT NUMBERS: Program Element 61153N24, Project RR024-03, Task Area RR024-03-02, Work Unit NR097-431
11. CONTROLLING OFFICE NAME AND ADDRESS: Office of Naval Research, 800 N. Quincy Street, Arlington, VA 22217	12. REPORT DATE: December 1980
	13. NUMBER OF PAGES: 77
14. MONITORING AGENCY NAME & ADDRESS(if different from Controlling Office)	15. SECURITY CLASS. (of this report): Unclassified
	15a. DECLASSIFICATION/DOWNGRADING SCHEDULE

16. DISTRIBUTION STATEMENT (of this Report)

Approved for public release; distribution unlimited

17. DISTRIBUTION STATEMENT (of the abstract entered in Block 20, if different from Report)

Same as Block NO. 16

18. SUPPLEMENTARY NOTES

19. KEY WORDS (Continue on reverse side if necessary and identify by block number)

Heat transfer, augmentation techniques, entropy generation, irreversibility, exergy.

20. ABSTRACT (Continue on reverse side if necessary and identify by block number)

The techniques for heat transfer augmentation play an important role in the development of efficient and inexpensive equipment for heat exchange processes. In the present study, the effectiveness of a given augmentation technique was determined based on the amount of irrversibility (waste of useful energy) introduced by the technique into the heat exchanger where it is to be used.

This report summarizes the main results obtained during the past two years under research contract N00014-79-C-0006 at the University of Colorado. The

DD FORM 1 JAN 73 1473 EDITION OF 1 NOV 65 IS OBSOLETE

Unclassified
SECURITY CLASSIFICATION OF THIS PAGE (When Data Entered)

report is organized into three distinct parts. The first part contains a fundamental investigation of the entropy generation mechanism in elementary heat transfer configurations. The second part describes in quantitative terms the irreversibility minimization potential of some of the most common augmentation techniques, namely, swirl-flow devices and roughened surfaces. The final part considers the entropy generation penalty associated with the use of extended surfaces (fins) in convective heat transfer. This part shows how the fin geometry may be selected so that the fin performs its prescribed heat transfer duty with minimum generation of entropy.

Report CUMER -80-9

EFFECTIVE TECHNIQUES FOR AUGMENTING HEAT TRANSFER: AN APPLICATION OF ENTROPY GENERATION MINIMIZATION PRINCIPLES

Final Report

December 1980

by

Adrian Bejan

Assistant Professor
Department of Mechanical Engineering
University of Colorado
Boulder, Colorado 80309

Prepared for

M.K. Ellingsworth
Program Monitor
The Office of Naval Research
Arlington, Virginia 22217

Under Contract No. N00014-79-C-0006, Work Unit 097-431

Table of Contents

1. INTRODUCTION

The growing emphasis on energy conservation has led to accelerated research on the development of efficient equipment for heat exchange processes. Today, a large share of this research is directed toward techniques for augmenting heat transfer [1.1-1.3]. The ultimate purpose of such techniques may be to improve the thermodynamic performance of future or existing heat exchangers, to reduce their size, thereby reducing capital and operating costs, and possibly, to prevent excessive temperatures and failure in systems where the heat generation rates are difficult to tolerate.

The task of evaluating the merit of a proposed augmentation technique may be as important as developing the technique itself. Experts agree that evaluating the impact of these techniques is a difficult problem [1.1-1.3], partly due to their great diversity and partly due to the absence of a common conceptual basis for evaluation. The present study was motivated by the real need for a universal, thermodynamically solid, basis for comparing the worth of all augmentation techniques.

In general, the objective of all heat transfer augmentation techniques is to enhance the thermal performance by increasing the surface heat transfer coefficient relative to the heat transfer coefficient which characterizes the standard (untouched) surface. At the same time, the increase in heat transfer coefficient should be accompanied by only a small increase in the fluid pumping power loss needed for the heat exchange job. These objectives underlie the fundamental trade-off in the development of any heat exchange equipment, namely, a design modification which improves the thermal contact will most likely cause a parallel increase in the mechanical power dissipated in the apparatus, for example the power needed for pumping the working fluid through the passages of a heat exchanger. Given this trade-off, it is important to know in advance

which augmentation technique will realistically lead to an improved overall performance. In addition to finding out whether an improvement is feasible, it is important to know, in quantitative thermodynamic terms, the size of the improvement.

This report summarizes the main results of a two-year study of the impact of heat transfer augmentation on the thermodynamic performance of heat exchange equipment. The study relied on the concept of thermodynamic irreversibility and entropy generation as fundamental criterion for evaluating and, eventually, minimizing the waste of usable energy (exergy) in energy systems. The extreme importance of this thermodynamic concept in the world of energy engineering was summarized most recently at the 1979 Second Law of Thermodynamics Workshop [1.4]. It has also been shown [1.3,1.5,1.6] that the ultimate function of all augmentation techniques is to inhibit the production of entropy, thus paving the road toward thermodynamically efficient equipment for heat exchange.

The work summarized in this report is organized into three distinct parts. The first part (section 2) contains a fundamental investigation of the entropy generation mechanism in elementary heat transfer configurations. This tutorial section establishes the foundation for the second law analysis of actual augmentation techniques, reported in sections 3 and 4. Section 3 describes in quantitative terms the irreversibility minimization potential of some of the most common techniques, namely, swirl-flow devices and roughened surfaces. Section 4 considers the entropy generation penalty associated with the use of extended surfaces (fins) in convective heat transfer. This section shows also how the fin geometry can be chosen such that the fin performs its heat transfer duty with minimum generation of entropy.

Due to space limitations, the present report reviews only a segment of the research undertaken during this two-year study. For a complete and detailed

account of all the topics covered by this study, the reader is encouraged to consult References [1.7-1.12].

References

1.1 A.E. Bergles, "Survey and Evaluation of Techniques to Augment Convective Heat and Mass Transfer," Progress in Heat and Mass Transfer, 1, 331-424 (1969).

1.2 A.E. Bergles, "Recent Developments in Convective Heat Transfer Augmentation," Applied Mechanics Reviews, 26, 675-682 (1973).

1.3 Summary Report of the "Research Workshop on Augmentation of Convective Heat Transfer (Encouraging or Accommodating High Heat Fluxes)," directed A.E. Bergles, April 22-23, 1974, Heat Transfer Laboratory, Department of Mechanical Engineering, Iowa State University (Report HTL-8, ISU-ERI-Ames-76026).

1.4 A.B. Cambel, G.A. Heffernan, D.W. Cutler and A. Ghamarian, editors, "Second Law Analysis of Energy Devices and Processes," Energy, 5, August-September 1980.

1.5 G.H. Junkhan, A.E. Bergles and R.L. Webb, Report HTL-21, ISU-ERI-Ames-80063, Iowa State University, Oct. 1979.

1.6 A. Bejan, Discussion on a previously published paper, J. Heat Transfer, 102, 586 (1980).

1.7 A. Bejan, "A Study of Entropy Generation in Fundamental Convective Heat Transfer," J. Heat Transfer, 101, 718-725 (1979).

1.8 W.R. Ouellette, "Entropy Generation Criterion Applied to Various Heat Transfer Augmentation Techniques," M.S. Thesis, Department of Mechanical Engineering, University of Colorado, Boulder, August 1979.

1.9 W.R. Ouellette and A. Bejan, "Conservation of Available Work (Exergy) by Using Promoters of Swirl Flow in Forced Convection Heat Transfer," Energy, 5, 587-596 (1980).

1.10 A. Bejan and P.A. Pfister, Jr., "Evaluating Heat Transfer Augmentation Techniques Based on their Impact on Entropy Generation," Letters in Heat and Mass Transfer, 7, 97-106 (1980).

1.11 A. Bejan, "Second Law Analysis in Heat Transfer," Energy, 5, 721-732 (1980).

1.12 D. Poulikakos, "Fin Geometry for Minimum Entropy Generation," M.S. Thesis, Department of Mechanical Engineering, University of Colorado, Boulder, December 1980.

2. ENTROPY GENERATION IN CONVECTIVE HEAT TRANSFER

2.1 Local Rate of Entropy Generation

Consider the two-dimensional infinitesimal fluid element dxdy shown schematically in Fig. 2.1. The fluid element is part of a considerably more complex convective heat transfer picture. However, for the scope of this study, we regard the element as an open thermodynamic system subjected to mass fluxes, energy transfer and entropy transfer interactions through a fixed control surface. The element size is small enough so that the thermodynamic state of the fluid inside the element may be regarded as uniform (independent of position). However, the thermodynamic state of the small fluid element may change with time.

For this study, we limit our attention to incompressible fluids without internal heat generation. In such cases, the expression for the volumetric rate of entropy generation reduces to [2.1]:

$$S''' = \frac{k}{T^2}\left[\left(\frac{\partial\theta}{\partial x}\right)^2 + \left(\frac{\partial\theta}{\partial y}\right)^2\right] + \frac{\mu}{T}\left\{2\left[\left(\frac{\partial v_x}{\partial x}\right)^2 + \left(\frac{\partial v_y}{\partial y}\right)^2\right] + \left(\frac{\partial v_x}{\partial y} + \frac{\partial v_y}{\partial x}\right)^2\right\} \quad (2.1)$$

As we might have expected, the irreversibility indicator S''' contains two additive parts, one due to conduction in the presence on non-zero temperature gradients, the other accounting for viscous dissipation of mechanical power throughout the flow. In the second term of equation (2.1), the factor in brackets represents the viscous dissipation function Φ for two-dimensional compressible flow.

The local entropy generation rate formula (2.1) can be derived in straightforward fashion by performing an entropy transfer accounting around the infinitesimally small element illustrated in Fig. 2.1. The entropy transfer

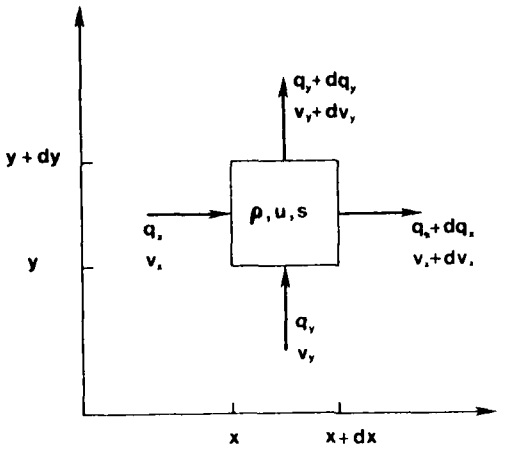

Fig. 2.1. Entropy generation analysis for an infinitesimal element dxdy in convective heat transfer.

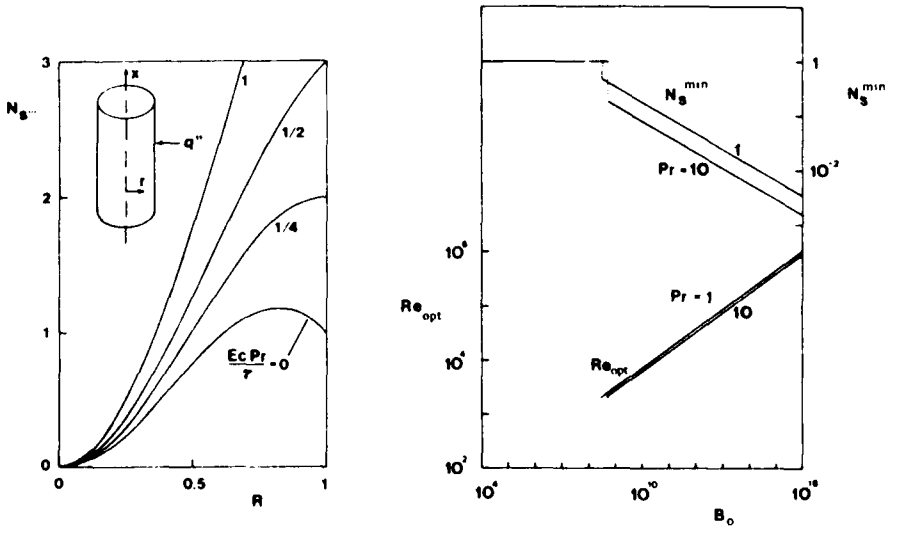

Fig. 2.2. Left: entropy generation profiles $N_{S'''}$ inside a smooth tube with constant wall heat flux in laminar flow. Right: optimum Reynolds number and corresponding minimum entropy generation number for forced convection heat transfer in a round tube.

to and from the (dxdy) system is associated with heat transfer, q_x and q_y, as well as with mass fluxes, ρv_x and ρv_y. In the interest of brevity we do not show this derivation, urging the reader to consult any irreversible thermodynamics book for additional details. Alternate versions of formula (2.1) corresponding to coordinate systems other than the two-dimensional cartesian system of Fig. 2.1 may be found in [2.2].

In many heat transfer problems it is often possible and convenient to neglect the viscous dissipation term $\mu\Phi$ in the equation for energy conservation.

$$\rho c_p \left(v_x \frac{\partial \theta}{\partial x} + v_y \frac{\partial \theta}{\partial y} \right) = k \left(\frac{\partial^2 \theta}{\partial x^2} + \frac{\partial^2 \theta}{\partial y^2} \right) + \mu\Phi \tag{2.2}$$

This is particularly the case in heat transfer through gases at subsonic velocities. The dimensionless group which expresses the magnitude of the dissipation energy term relative to the conduction energy term in (2.2) is [2.3]

$$\text{Ec Pr} = \frac{u^{*2}}{c_p \theta^*} \quad \frac{\nu}{\alpha} \tag{2.3}$$

where u^* and θ^* are the characteristic fluid velocity and temperature difference for the convective heat transfer problem. Thus, in many engineering problems, we find $\text{Ec Pr} << 1$.

Consider now the same question relative to expression (2.1). Under what conditions is the viscous dissipation contribution to S''' negligible? If we regard expression (2.1) as the sum $S''' = S'''_{\text{conductive}} + S'''_{\text{viscous}}$, then, in an order of magnitude sense,

$$O\left(\frac{S'''_{\text{viscous}}}{S'''_{\text{conductive}}} \right) = \frac{\text{Ec Pr}}{\tau} \tag{2.4}$$

Here, $\tau = \theta^*/T^*$, where T^* is the absolute temperature characteristic to the problem at hand. The dimensionless temperature difference, τ, is always an important dimensionless parameter in second law analyses of heat transfer problems. With the exception of applications at cryogenic temperatures, the temperature difference number τ is generally much smaller than unity, $\tau << 1$.

It is now clear that the energy argument by which viscous dissipation is neglected in (2.2), i.e., $Ec\ Pr << 1$, has no bearing on the question of negligible viscous contribution to the local rate of irreversibility production. It is then possible to encounter situations where, although the energy equation can be simplified according to $Ec\ Pr << 1$, S''' is in fact dominated by viscous effects. This is the limit in which τ is very small, small enough so that $Ec\ Pr/\tau > 1$.

Below we examine a series of important convective heat transfer configurations in an effort to illustrate the coupling of viscous and conductive effects in the makeup of S'''. In the process we will study the spatial distribution of irreversibility, pointing out those flow features which act as concentrators (sources) of entropy generation S'''.

2.2 Forced Convection in a Round Tube

Laminar Flow. Consider the Poiseuille flow through a round tube with uniform heat flux q'' around its circumference (see insert in the left side of Fig. 2.2). The velocity and temperature profiles for this flow are particularly simple [2.2]:

$$v_x = v_{x,max}\left[1 - \left(\frac{r}{r_o}\right)^2\right] \tag{2.5}$$

$$0 = \frac{q''r_o}{k}\left[-4\,\frac{x}{x_o} - \left(\frac{r}{r_o}\right)^2 + \frac{1}{4}\left(\frac{r}{r_o}\right)^4\right] \tag{2.6}$$

with

$$v_{x,max} = \frac{r_o^2}{4}\left(-\frac{dP}{dx}\right), \quad \frac{x_o}{r_o} = \frac{r_o v_{x,max}}{\alpha} = Pe\,. \tag{2.7,8}$$

The equation for S''' in the cylindrical geometry of Fig. 2.2 is

$$S''' = \frac{k}{T^2}\left[\left(\frac{\partial\theta}{\partial x}\right)^2 + \left(\frac{\partial\theta}{\partial r}\right)^2\right] + \frac{\mu}{T}\left(\frac{\partial v_x}{\partial r}\right)^2 \tag{2.9}$$

which yields

$$S''' = \frac{q''^2}{kT^2}\left[(2R - R^3)^2 + \frac{16}{Pe^2}\right] + \frac{4\mu v_{x,max}^2}{Tr_o^2}\,R^2\,, \quad R = \frac{r}{r_o} \tag{2.10}$$

Equation (2.10) is the entropy generation profile in the pipe cross-section. Together with the velocity and temperature profiles, the entropy generation profile completes the thermodynamic description of the convective heat transfer phenomenon.

It is convenient to nondimensionalize expression (2.10) and define the local entropy generation number $N_{S'''}$

$$N_{S'''} = S'''\,\frac{kT_o^2}{q''^2} = (2R - R^3)^2 + \frac{16}{Pe^2} + \frac{4\,Ec\,Pr}{\tau}\,R^2\,. \tag{2.11}$$

Here we made the assumption that the temperature variation over the pipe cross-section is negligible compared with the absolute temperature, hence $T \approx T_o$ where T_o is a characteristic (reference) absolute temperature. The irreversibility figure $N_{S'''}$ depends on radial position, on Pe and on the

group $Ec\ Pr/\tau$ which, as discussed in the preceding section, determines the relative importance of viscous effects. The Peclet number Pe governs the importance of irreversibility associated with conduction in the axial direction. We see that for $Pe < 4$ the axial conduction contribution dominates the radial conduction effect.

The left side of Fig. 2.2 displays a family of entropy generation profiles in the pipe cross-section, for cases where the axial conduction effect is negligible ($Pe >> 4$). The value of $Ec\ Pr/\tau$ increases gradually to the point where viscous effects dominate $N_{S'''}$. In all cases, the pipe wall region acts as a strong concentrator of irreversibility. When $Ec\ Pr/\tau = 0$, the maximum $N_{S'''}$ occurs inside the fluid at $R = (2/3)^{1/2}$, the same place where due to the wall curvature effect the maximum radial temperature gradient is located. As viscous effects take over, the point of highest $N_{S'''}$ migrates toward the wall and, for $Ec\ Pr/\tau > 1/4$, it coincides with the wall.

The rate of entropy generation over the entire tube cross-section is obtained by integrating expression (2.10),

$$S' = 2\pi\, r_o^2 \int_0^1 S'''\ R\ d\ R\,. \tag{2.12}$$

Neglecting axial conduction, $Pe >> 4$, result (2.12) can be written as

$$S' = \frac{11}{48\pi}\,\frac{q'^2}{kT^2} + \frac{8}{\pi}\,\frac{\mu \dot{m}^2}{T\rho^2\, r_o^4}\,, \tag{2.13}$$

Here $\dot{m}$ is the mass flow rate through the tube, while q' is the heat transfer rate per unit length, $2\pi r_o q''$. Once more, the irreversibility production S' appears as the sum of two effects, heat transfer in the direction of a finite temperature gradient and fluid friction. It should be noted that the heat transfer

contribution to S', the first term in equation (2.13), is fixed as soon as the heat transfer rate per unit length q' (the heat transfer duty of the tube) is specified. We return to this observation later in this section when we address the question of optimum tube radius for minimum irreversibility and fixed q'.

Turbulent Flow. Exact analytical solutions for the turbulent velocity and temperature fields in the tube cross-section are not available. Therefore, one cannot evaluate the rate of entropy generation at any point in the pipe cross-section, as done through equation (2.10) for laminar flow. However, one can still evaluate the rate of entropy generation averaged over the tube cross-section by using the integral result developed by Bejan [2.4] for irreversibility in a duct of arbitrary geometry.

Using the present notation for forced convection through a tube, the integral result is [2.4]

$$S' \frac{1}{\pi \, Nu} \frac{q'^2}{kT^2} + \frac{\dot{m}^3 f}{\rho^2 T \, r_o^5} \quad , \tag{2.14}$$

which shows how S' can be evaluated based on average heat transfer (Nu) and fluid friction (f) information. As one might expect, the laminar flow expression (2.13) is only a special case of the more general result (2.14) since, in laminar flow, $Nu = 48/11$ and $f = 8 \pi \mu r_o/\dot{m}$. Unlike in laminar flow, the heat transfer contribution to S' is not necessarily constant when the heat transfer duty q' is specified.

Optimum Tube Radius for Minimum Irreversibility. In an application in which the heat transfer duty q' and the mass flow $\dot{m}$ are already specified, it is possible to select an optimum tube radius which insures the minimum rate of entropy generation in the heat transfer device. This design optimization

procedure is described best by placing the irreversibility rate expression (2.14) in dimensionless form. We define the entropy generation number N_S' as the ratio $S'/S'_{\Delta T,laminar}$ where S' is the actual entropy generation rate given by (2.14) and $S'_{\Delta T,laminar}$ is the first term appearing in (2.13). We commented earlier that $S'_{\Delta T,laminar}$ is constant when the heat transfer rate q' is specified, hence, $S'_{\Delta T,laminar}$ assumes the role of characteristic rate of entropy generation in the system of interest.

The entropy generation number is therefore

$$N_{S'} = \frac{48}{11} Nu^{-1} + \frac{3\pi^4}{22} f\, Re^5\, B_o^{-2} , \qquad (2.15)$$

showing that the duct irreversibility depends primarily on two dimensionless groups, the Reynolds number based on tube diameter Re and the "duty" parameter B_o,

$$Re = \frac{2\dot{m}}{\rho\mu r_o} ; \quad B_o = q'\dot{m} \frac{\rho}{\mu^{5/2}(kT)^{1/2}} . \qquad (2.16,17)$$

With q', $\dot{m}$ and working fluid specified, the task of finding the optimum radius for minimum S''' is equivalent to minimizing the N_S' expression (2.15) with respect to Re, subject to a specified constant B_o. This procedure is straightforward, therefore only the final results are given here.

For laminar flow, using $Nu = 48/11$ and $f = 16/Re$ in expression (2.15), the minimization procedure yields

$$Re_{opt} = 0 ; \quad N_{S'}^{min} = 1 \qquad (2.18,19)$$

In engineering terms, this result implies that the selected tube radius r_o must be large enough so that the rate of entropy generation is strongly dominated by the contribution due to heat transfer across a finite temperature

difference. In other words, based on expression (2.15),

$$\frac{24\pi^4}{11} Re^4 B_o^{-2} << 1 \quad . \tag{2.20}$$

For turbulent flow, the $N_{S'}$ expression (2.15) has a unique minimum. Substituting $Nu = 0.023\ Pr^{0.4} Re^{0.8}$ and $f = 0.046\ Re^{-0.2}$ into (2.15) and differentiating with respect to Re yields

$$Re_{opt} = 2.023\ Pr^{-0.071} B_o^{-0.358} \tag{2.21}$$

and

$$N_{S'}^{min} = 126\ Pr^{-0.343} B_o^{-0.286} \quad . \tag{2.22}$$

Expressions (2.21, 22) have been summarized in the right hand side of Fig. 2.2 for two discrete values of Prandtl number. As the aggregate duty parameter B_o increases, we see that the optimum tube radius decreases (Re_{opt} increases) and the minimum entropy generation number N_S^{min} decreases also.

2.5 Boundary Layer Over Flat Plate

Laminar Flow over Isothermal Plate. Consider now the development of laminar momentum and thermal boundary layers along a flat plate. The situation is shown schematically in the horizontal plane of the isometric drawing of Fig. 2.3. At some distance from the solid wall the fluid velocity and temperature are uniform, $u_{x,\infty}$ and T_∞. The wall temperature is constant, T_o.

The study of the velocity and temperature fields in the vicinity of the plate constituted the subject of numerous investigations [2.5]. The purpose of this section is to examine the distribution of entropy generation in the boundary layer. For this we rely on solutions available in the literature for

$v_x(x,y)$ and $\theta(x,y)$ in laminar flow.

The task of evaluating the entropy generation profile S''' is simplified greatly if we restrict the discussion to the case $Pr = 1$ for which the Blasius-Pohlhausen solution [2.6] reduces to

$$\frac{\theta}{\theta_\infty} = \frac{v_x}{v_{x,\infty}} = \frac{df}{d\eta} \tag{2.23,24}$$

The similarity variable η equals $y[v_{x,\infty}/(\nu x)]^{1/2}$, while $f(\eta)$ is the function tabulated by Howarth [2.7]. Neglecting the irreversibility terms associated with velocity and temperature gradients in x direction, we find

$$S''' = \frac{k\theta_\infty^{\,2} v_{x,\infty}}{T_o^{\,2}\nu x}(f'')^2 + \frac{\mu v_{x,\infty}^{\,3}}{T_o \nu x}(f'')^2 \tag{2.25}$$

The local entropy generation number is

$$N_{S'''} = \frac{S'''}{k}\left(\frac{\nu T_o}{\theta_\infty v_{x,\infty}}\right)^2 = \left(1 + \frac{Ec\ Pr}{\tau}\right)\frac{(f'')^2}{Re_x}, \quad Pr = 1, \tag{2.26}$$

where Re_x is defined as $v_{x,\infty}x/\nu$.

The complex dependence of S''' on both x and y is shown in Fig. 2.3. The three-dimensional display was done in terms of $(x\ v_{x,\infty}/\nu)$ and $(y\ v_{x,\infty}/\nu)$ in the horizontal plane, and $N_{S'''}/(1 + Ec\,Pr/\tau)$ in the vertical direction. It is evident that the irreversibility effects are limited to the boundary layer. Regarding the y dependence of $N_{S'''}$, the entropy generation rate is highest reaching a peak at the solid wall. The longitudinal variation of S''' is as $1/x$, indicating that like all gradients in this boundary layer solution S''' blows up at the origin. The viscous effect again scales up as $Ec\ Pr/\tau$.

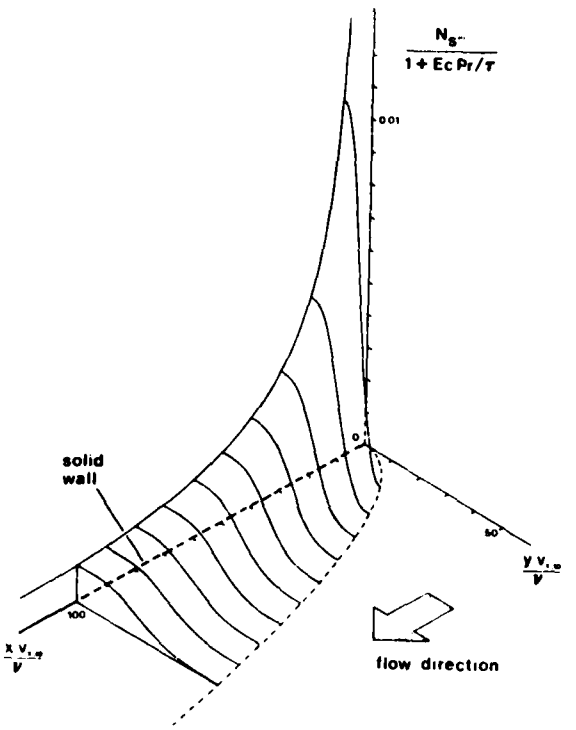

Fig. 2.3. Entropy generation surface for laminar boundary layer flow and heat transfer along a flat plate.

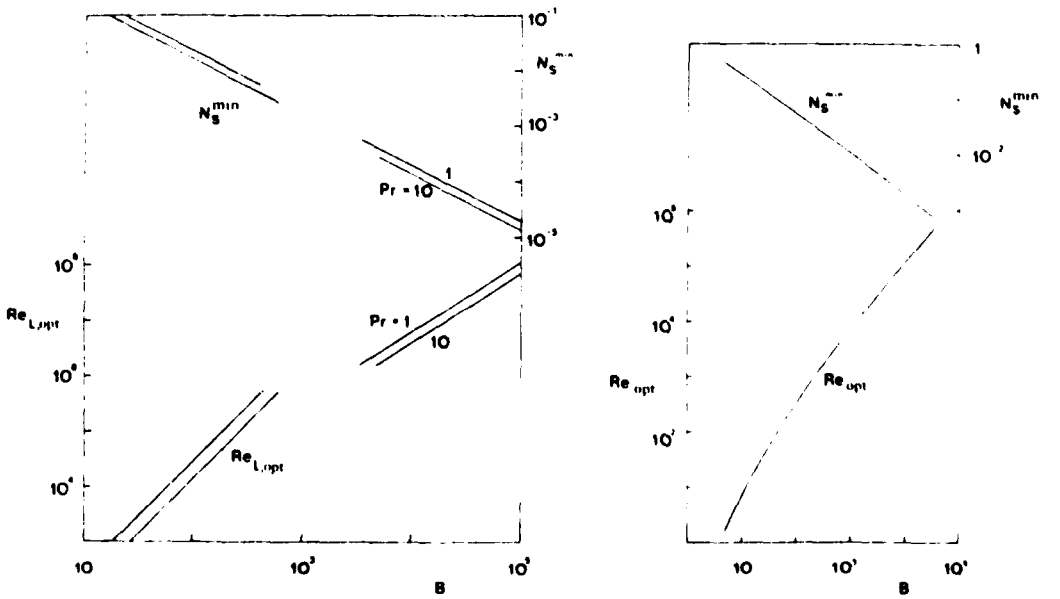

Fig. 2.4. Optimum Reynolds number and corresponding minimum entropy generation number. Left: boundary layer flow over a flat plate. Right: single cylinder in gaseous cross-flow.

Integrating (2.25) across the boundary layer we can calculate the rate of entropy generation per unit area of flat plate,

$$S'' = \int_0^\infty S''' \, dy = 0.25 \, \frac{k v_{x,\infty} \theta_\infty^2}{\nu T_o^2} \left(1 + \frac{Ec \; Pr}{\tau} \right) Re_x^{-1/2} \tag{2.27}$$

with the corresponding entropy generation number defined as

$$N_{S''} = S'' \, \frac{\nu T_o^2}{k v_{x,\infty} \theta_\infty^2} = 0.25 \left(1 + \frac{Ec \; Pr}{\tau} \right) Re_x^{-1/2} \, . \tag{2.28}$$

Finally, by analogy with the Nusselt number nomenclature for boundary layer heat transfer, we integrate (2.27) in the x direction to find the total rate of entropy generation produced by boundary layer flow and heat transfer over a length L

$$S' = \int_0^L S'' \, dx = 0.50 \, \frac{k \theta_\infty^2}{T_o^2} \left(1 + \frac{Ec \; Pr}{\tau} \right) Re_L^{1/2} \tag{2.29}$$

where $Re_L = v_{x,\infty} L/\nu$. The overall entropy generation number based on S' is

$$N_{S'} = S' \, \frac{T_o^2}{k \theta_\infty^2} = 0.50 \left(1 + \frac{Ec \; Pr}{\tau} \right) Re_L^{1/2} \, . \tag{2.30}$$

It is worth mentioning that in general the Prandtl number will have an additional effect on the relative importance of viscous and conductive effects in the constitution of S''', S'' and S'. It is easy to show that when $Pr \neq 1$ the viscous effects scale as

$$\frac{Ec \; Pr}{\tau} \left(\frac{\delta_T}{\delta} \right)^2 \sim \frac{Ec \; Pr^{1/3}}{\tau} \tag{2.31}$$

where δ and δ_T are the velocity and temperature boundary layer thicknesses. In writing (2.31) we made use of the approximation $\delta/\delta_T \approx Pr^{1/3}$. The significance of (2.31) is that when the two thicknesses are not equal, the thinner layer exhibits larger gradients thereby enhancing its contribution to the total S''' figure. According to (2.31), viscous effects are more likely to play a role in low Prandtl number fluids where $\delta << \delta_T$.

Laminar and Turbulent Flow over Constant Heat Flux Plate. To study the generation of entropy in a turbulent boundary layer one has to rely on an integral method which takes into account the heat transfer and fluid friction characteristics of the flow in an overall manner, as Nusselt number and friction factor information. Consider, for example, a flat plate of negligible thickness suspended in a uniform flow field, parallel to the flow velocity $v_{x,\infty}$. The heat flux q" over the plate surface is uniform. Consider also a control surface which surrounds the plate of finite length L at a large enough distance through portions of external flow in which the fluid motion is nearly uniform and the temperature nearly constant, T_∞. Regardless of whether the boundary layer is turbulent or laminar, the entropy generation rate in one half of the control volume (i.e., for one side of the plate) is given by

$$S' = \frac{q''^2}{T_\infty} \int_0^L \frac{dx}{h_x} + \frac{\rho v_{x,\infty}^3}{2\, T_\infty} \int_0^L C_{f,x}\, dx \ , \qquad (2.32)$$

where h_x and $C_{f,x}$ are the local heat transfer coefficient and skin friction coefficient,

$$h_x = \frac{q''}{T_o(x) - T_\infty} \ , \quad C_{f,x} = \frac{2\,\tau_o}{\rho v_{x,\infty}^2} \qquad (2.33,34)$$

In the above definitions $T_o(x)$ is the wall temperature, τ_o the wall shear stress and q'' the uniform heat flux. Note that unlike equation (2.29) in the preceding sub-section where we considered the laminar boundary layer over an isothermal flat plate, the S' expression (2.32) refers to a uniform heat flux situation.

Expression (2.32) is the result of an entropy flux accounting around the control volume, analysis omitted here due to space limitations. Like all entropy generation results for forced convection heat transfer, S' consists of two additive parts, one due to heat transfer across the $[T_o(x) - T_\infty]$ temperature difference, the other being associated with the total friction drag force exerted by the fluid on the plate. Below, we use result (2.32) to determine the optimum plate length L which yields the minimum rate of entropy generation in a heat transfer application in which the uniform flow velocity $v_{x,\infty}$ and the total heat flux $q' = \int_0^L q'' \, dx$ are specified. We do this by first substituting appropriate correlations for h_x and $C_{f,x}$ into expression (2.32) and solving the equation $\partial S'/\partial L = 0$.

For laminar flow, the local skin friction coefficient is $C_{f,x} = 0.664 \, Re_x^{-1/2}$ while the local heat transfer coefficient is given by $h_x x/h = 0.332 \, Pr^{1/3} \, Re_x^{1/2}$ [2.8]. Writing $q' = q''L$ for the total heat transfer rate from plate to fluid over the plate length L, the entropy generation number $N_{S'}$ becomes

$$N_{S'} = S' \frac{kT_\infty^2}{q'^2} = 2.008 \, Pr^{-1/3} Re_L^{-1/2} + 0.664 \, Re_L^{1/2} \, B^{-2} . \qquad (2.35)$$

Here, Re_L and B are the Reynolds number based on L and the "duty" parameter, respectively,

$$Re_L = \frac{v_{x,\infty} L}{\nu} \quad , \quad B = \frac{q'}{v_{x,\infty} (\mu k T)^{1/2}} . \qquad (2.36,37)$$

The optimum plate length $Re_{L,opt}$ yielding the minimum rate of entropy generation at constant q' and $v_{x,\infty}$ is

$$Re_{L,opt} = 3.024\ Pr^{-1/3}\ B^{2}, \quad N_{S'}^{min} = 2.309\ Pr^{-1/6}\ B^{-1}. \qquad (2.38,39)$$

For turbulent flow we use a similar set of correlations for friction and heat transfer $C_{f,x} = 0.0576\ Re_x^{-1/5}$ and $h_x\ x/k = 0.0296\ Pr^{1/3}\ Re_x^{0.8}$ [15]. We also assume that the laminar layer which precedes the turbulent boundary layer is much shorter than the plate length L. Substituting these correlations into the entropy generation result (2.32) yields

$$N_{S'} = S'\ \frac{kT_\infty^{\,2}}{q'^2} = 28.15\ Pr^{-1/3}\ Re_L^{8/5} + 0.036\ Re_L^{-8/5}\ B^{-2}, \qquad (2.40)$$

$$Re_{L,opt} = 64.31\ Pr^{-5/24}\ B^{5/4}, \quad N_{S''}^{min} = 2.013\ Pr^{-1/6}\ B^{-1}. \qquad (2.41,42)$$

The optimum plate length and the resulting minimum entropy generation number prescribed by these equations are shown on the left side of Fig. 2.4. The discontinuity illustrated by dashed lines corresponds to the transition region, cases in which the laminar and turbulent portions of the boundary layer are of comparable lengths. The trends are similar to those presented in the right graph of Fig. 2.2: the higher the duty parameter B, the higher the optimum Reynolds number (plate length) and the lower the minimum entropy generation number. In other words, if the total heat transfer rate q' is constant and the flow velocity increases, the optimum plate length decreases and the minimum attainable entropy generation rate increases.

These conclusions are applicable to the optimization of local flow geometry in plate-fin surfaces for compact heat exchangers, as shown in Chapter 4 of this report.

2.4 Single Cylinder in Cross-Flow

The heat transfer between a cylindrical surface and a fluid flow normal to the cylinder axis is one of the most frequent heat transfer configurations encountered in actual engineering equipment for heat exchange processes. It is appropriate to examine here the thermodynamic irreversibility introduced by this configuration. Due to inherent similarities with the plate of finite length in parallel boundary layer flow, example concluded in the preceding section, the case of a single cylinder in cross-flow will be summarized very briefly and only the key analytical results will be given.

Consider a cylinder of diameter D with uniform surface heat flux q'' in a cross-flow of uniform velocity $v_{x,\infty}$ and temperature T_∞. An entropy generation analysis of the flow region affected by heat and momentum transfer from the cylinder yields the total entropy generation rate

$$S' = \frac{q''}{T_\infty^2} \oint [T(\ell) - T_\infty] \, d\ell + \frac{v_{x,\infty} F_D}{T_\infty} \quad . \tag{2.43}$$

In this expression, ℓ is the curvilinear coordinate around the cylindrical surface and $T(\ell)$ is the local surface temperature. It is again assumed that the temperature differences are much smaller than the characteristic absolute temperature of the medium $[T(\ell) - T_\infty] << T_\infty$. F_D is the force (drag) per unit length exerted by flow on cylinder, force calculated from drag coefficient experimental information, C_D,

$$C_D = \frac{F_D/D}{\rho v_{x,\infty}^2/2} \quad . \tag{2.44}$$

Replacing the line integral in (2.43) with the average wall-fluid temperature difference times πD, and expressing the average temperature difference in terms

of the average Nusselt number, $T(\ell)_{av} - T_\infty = q''D/(k\,Nu)$, yields,

$$S' = \frac{q'^2}{\pi k T_\infty^2}\frac{1}{Nu} + \frac{1}{2} C_D\, Re\, \frac{\mu v_{x,\infty}^2}{T_\infty} . \qquad (2.45)$$

Here, we used the drag coefficient to replace F_D in equation (2.43). We also wrote $q' = \pi D q''$ for the total heat transfer rate per unit length of cylinders. Finally, expression (2.45) is put in dimensionless form defining the entropy generation number

$$N_{S'} = S' \frac{kT_\infty^2}{q'^2} = \frac{1}{\pi Nu} + \frac{1}{2} C_D\, Re\, B^{-2} , \qquad (2.46)$$

where B is a duty parameter which has the same form as in equation (2.37).

As in the heat transfer configurations examined earlier, we can use the entropy generation number formula (2.46) to determine which flow geometry (cylinder diameter D) is best for minimizing the thermodynamic losses associated with the heat transfer process. For an application in which q', $v_{x,\infty}$ and the fluid are known, the optimization procedure amounts to minimizing expression (2.46) with respect to Re, subject to constant B. The results of this optimization procedure are shown as Re_{opt} and $N_{S'}^{min}$ on the right side of Fig. 2.4, a plot qualitatively similar to the left graph obtained for a flat plate. The right graph of Fig. 2.4 was constructed based on equation (2.46) coupled with Hilpert's average Nusselt number correlation for gas flow [2.9] and with Eisner's presentation of drag coefficient [2.10].

2.5 Laminar Forced Convection in the Entrance Region of a Flat Rectangular Duct

A frequent flow configuration which embodies the characteristics of the first two flow examples discussed here is sketched in the insert of Fig. 2.5. In the entrance region of a parallel-plate duct, temperature and velocity boundary

layers develop simultaneously along both walls, gradually filling the duct and leading to the well-known fully-developed laminar regime. There have been many studies of the heat transfer and velocity problems associated with this basic configuration, as indicated recently by Bhatti and Savery [2.11]. In this section we address the irreversibility problem, once again relying on published solutions for the temperature and velocity field in the duct.

Sparrow [2.12] analyzed the boundary layer development in the entrance region using the Karman-Pohlhausen integral technique. The Sparrow solution is unique, considering its simplicity versus the good agreement between its predictions and experimental findings. In what follows we use this solution and the S''' formula (2.1) to illustrate the distribution of irreversibility in the channel.

The ultimate goal of the irreversibility analysis is to discover how the thermodynamic losses due to entrance effects compare with similar losses in the fully-developed section of the duct. In other words, what length of fully-developed flow is guilty of generating as much entropy as the entire entrance region? The answer to this question is simplified substantially if, in addition to using Sparrow's analytical solution, we focus on the $\tau \to 0$ limit in which the viscous effects totally dominate the rate of entropy generation in the channel (see the discussion following equation (2.4)). Consequently, to calculate S''' we need only the velocity solution which is

$$v_x = V_o V_1^*(2\xi - \xi^2) \tag{2.47}$$

with

$$\xi = y/\delta\ ,\quad \delta/a = 3(1 - V_1^{*-1}) \tag{2.48,49}$$

$$V_1^* = V_1/V_o\,, \quad x^* = \frac{x\nu}{a\,V_o}\,. \tag{2.50,51}$$

As shown on Fig. 2.5, V_o is the uniform fluid velocity at $x = 0$, while V_1 and δ are the centerline velocity and boundary layer thickness, respectively. For the function $V_1^*(x^*)$, Sparrow reports a differential equation which, integrated, yields

$$x^* = \frac{3}{10}\left(9V_1^* - 2 - \frac{7}{V_1^*} - 16\ \ell n\ V_1^*\right) \tag{2.52}$$

The entrance region extends to $x^* = 0.1038$, corresponding to $V_1^* = 3/2$ as for plane Poiseuille flow.

Using equation (2.1) and leaving out the conductive contribution we obtain

$$S''' = \frac{4\mu\ V_o^2}{T\delta^2}\ V_1^{*2}(1-\xi)^2 \tag{2.53}$$

and, integrating across the duct,

$$S'' = 2\int_0^a S'''\,dy = \frac{8}{3}\,\frac{\mu V_o^{\ 2}}{T\delta}\ V_1^{*2}\,. \tag{2.54}$$

From (2.54) we find that in the fully-developed section of the duct (FD) the rate of entropy generation per unit area of duct wall is

$$S''_{FD} = 6\,\frac{\mu V_o^{\ 2}}{Ta}\,. \tag{2.55}$$

Fig. 2.6 shows the variation of S''/S''_{FD} with axial position along the duct. As expected, the irreversibility effects are most intense near $x = 0$. However, as x^* increases, S'' rapidly approaches the fully-developed entropy generation

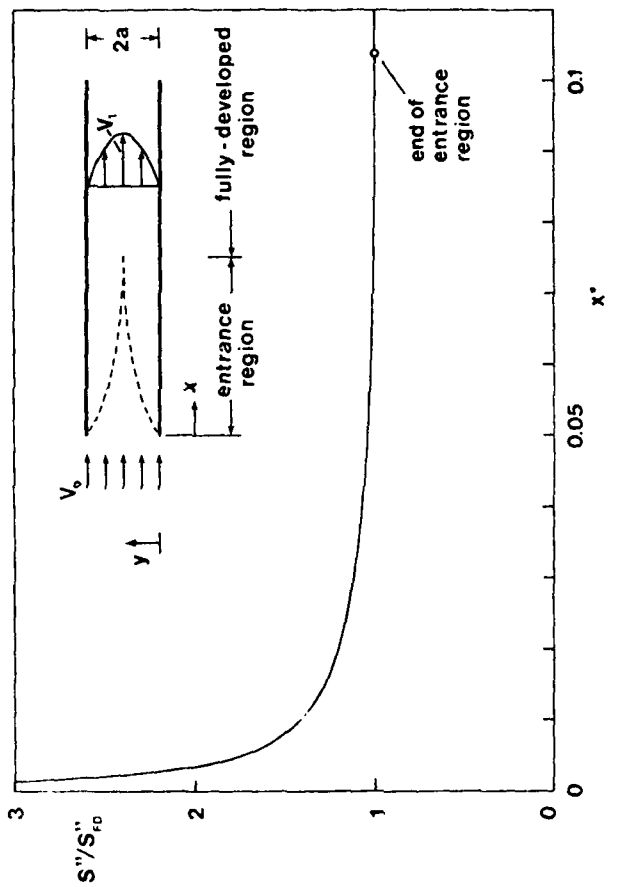

Fig. 2.5. Distribution of the entropy generation rate in the entrance region of a flat rectangular duct in laminar flow.

level S''_{FD} a good distance before the end of the entrance region, $x^* = 0.1038$.

The total irreversibility associated with entrance effects is estimated integrating expression (2.54) from $x^* = 0$ to $x^* = 0.1038$. The result of this operation is

$$S' = \frac{11}{15} \frac{\rho a V_o^3}{T} \tag{2.56}$$

where ρ is the fluid density. Similarly, the total rate of entropy generation over a fully-developed stretch of length L_{FD} is

$$S'_{FD} = 6 \frac{\mu V_o^2}{Ta} L_{FD} \ . \tag{2.57}$$

Comparing results (2.56) and (2.57), we conclude that the fully-developed equivalent of the entire entrance region is a fully-developed section of length L_{FD} given by

$$\frac{L_{FD}}{D} = \frac{11}{1440} Re_D = 0.00764 \ Re_D \ , \tag{2.58}$$

where D is the hydraulic diameter $4a$, while $Re_D = V_o D/\nu$. It is time now to compare the irreversibility-equivalent length L_{FD} with the physical extent of the entrance region, L_E. Setting $x^* = 0.1038$ and $x = L_E$ in expression (2.51) we find that familiar result

$$\frac{L_E}{D} = 0.00649 \ Re_D \ . \tag{2.59}$$

Therefore, from (2.58,59), the irreversibility contributed by the entrance region is roughly equal to (actually, only about 18% higher than) the irreversibility estimated assuming fully-developed flow over a duct length equal to the entrance

length. This conclusion is important in practical irreversibility calculations, as it is considerably easier to treat the entire duct as in the fully-developed regime.

References

2.1 Kestin, J., A Course in Thermodynamics, Vol. II, Blaisdell, Waltham, Massachusetts, 1968, p. 433.

2.2 Bird, R.B., Stewart, W.E. and Lightfoot, E.N., Transport Phenomena, Wiley, New York, 1960.

2.3 Kestin, J. and Richardson, P.D., Int. J. Heat Mass Transfer, Vol. 6, 1963, p. 147.

2.4 Bejan, A., Int. J. Heat Mass Transfer, Vol. 21, 1978, p. 655.

2.5 Schlichting, H., Boundary Layer Theory, 6th Edition, McGraw-Hill, New York, 1968.

2.6 Pohlhausen, E.Z., Zeitschrift für angewandte Mathematik und Mechanik, Vol. 1, 1921, p. 115.

2.7 Howarth, L., Proceedings of the Royal Society of London, Series A. Vol. 164, 1938, p. 547.

2.8 Rohsenow, W.M. and Choi, H.Y., Heat, Mass and Momentum Transfer, Prentice-Hall, Englewood Cliffs, 1961, pp. 39, 148.

2.9 Hilpert, R., Forsch. Geb. Ingenieur, Vol. 4, 1933, p. 215.

2.10 Eisner, F., 3rd Int. Cong. App. Mech., Stockholm, 1930, also in Rohsenow, W.M. and Choi, H.Y., Op. Cit., p. 79.

2.11 Bhatti, M.S. and Savery, C.W., ASME Journal of Heat Transfer, Vol. 100, Aug. 1978, p. 539.

2.12 Sparrow, E.M., NACA TN 3331, 1955.

Nomenclature

a	half-thickness of flat duct
B_o, B	duty parameters
c_p	specific heat at constant pressure
C_D	drag coefficient
$C_{f,x}$	local skin friction coefficient
D	hydraulic diameter
Ec	Eckert number
f	function, equation (2.26); friction factor, equation (2.14)
F_D	drag force
h_x	local heat transfer coefficient
k	thermal conductivity
L_E	entrance region length
L_{FD}	length of irreversibility-equivalent fully developed section
$\dot{m}$	mass flow rate
$N_{S'''}$, $N_{S''}$, $N_{S'}$	entropy generation number
Nu	Nusselt number
P	pressure
Pr	Prandtl number
q" , q' , q	heat transfer interaction, [W/m^2], [W/m], [W]
r	radial position
r_o	tube radius
R	dimensionless radial position
Re	Reynolds number
s	specific entropy
S''' , S", S'	rate of entropy generation, [W/m^{3}K], [W/m^{2}K], [W/mK]

S''_{FD}	rate of entropy generation in the fully-developed region
t	time
T	absolute temperature
T_o	reference temperature
u	specific internal energy
v_x, v_y	velocity components
V_o	entrance velocity
V_o	centerline velocity
V_1^*	dimensionless centerline velocity
x	horizontal coordinate
x^*	dimensionless coordinate
y	vertical coordinate
α	thermal diffusivity
δ	velocity boundary layer thickness
δ	thermal boundary layer thickness
ζ	dimensionless coordinate across flat duct
η	similarity variable in boundary layer flow over flat plate
θ	temperature difference, $T - T_o$
θ_∞	extreme temperature difference, $T_\infty - T_o$
μ	viscosity
ν	kinematic viscosity
ρ	fluid density
τ	ratio of characteristic temperature difference divided by the absolute temperature
τ_o	wall shear stress
Φ	viscous dissipation function

3. THE IMPACT OF HEAT TRANSFER AUGMENTATION ON ENTROPY GENERATION

3.1 Entropy Generation Analysis

Consider a heat-exchanger passage of length dx, heat transfer per unit length q', and mass flowrate $\dot{m}$. The passage geometry is described in terms of the hydraulic diameter D and flow cross sectional area A. The rate of entropy generation per unit length is [3.1]

$$S' = \frac{q'\Delta T}{T^2} + \frac{\dot{m}}{\rho T}\left(-\frac{dP}{dx}\right) \tag{3.1}$$

where the first term represents the irreversibility rate due to heat transfer across the wall-fluid temperature difference, $S'_{\Delta T}$, while the second term is the irreversibility rate attributed to fluid friction, $S'_{\Delta P}$. Implicit in writing Eq. (3.1) is the assumption that the wall-fluid ΔT is considerably smaller than the local (wall, fluid) absolute temperature. This is a good assumption, especially in heat exchangers operating above room temperature.

An important dimensionless parameter in the second law analysis of convective heat transfer is the irreversibility distribution ratio

$$\phi = S'_{\Delta P}/S'_{\Delta T}. \tag{3.2}$$

The parameter ϕ describes the relative importance of fluid friction in the total irreversibility of a flow passage. Like $S'_{\Delta P}$ and $S'_{\Delta T}$, the irreversibility distribution ratio ϕ is a local parameter.

The impact of an augmentation technique on the irreversibility of a given heat exchanger passage can be evaluated by calculating the entropy generation rate in the "augmented" passage, S'_a, and comparing it with the entropy

generation rate in the original (unaugmented) passage, S'_o. It is convenient to define the augmentation entropy generation number $N_{S,a}$ as the ratio

$$N_{S,a} = S'_a/S'_o . \tag{3.3}$$

Augmentation techniques yielding values of $N_{S,a}$ less than unity are thermodynamically advantageous since, in addition to enhancing heat transfer, they reduce the rate of entropy generation in the apparatus.* It is easy to show that when q' and $\dot{m}$ are the same before and after augmentation, the entropy generation number can be rewritten as

$$N_{S,a} = (N_T + \phi_o N_p)/(1 + \phi_o) , \tag{3.4}$$

where

$$N_T = (St_o/St_a)(D_a/D_o) , \tag{3.5}$$

$$N_p = (f_a/f_o)(D_o/D_a)(A_o/A_a)^2 , \tag{3.6}$$

$$Re_a = (D_a A_o/D_o/A_a) Re_o . \tag{3.7}$$

In these expressions, St, f, Re, D and A are the Stanton number, friction factor, and Reynolds number, hydraulic diameter and flow cross sectional area,

* For example, in the regenerative heat exchanger for a Brayton cycle heat engine a low $N_{S,a}$ means less dissipation of available work in the power cycle. Among the physical parameters affected directly are the stream-to-stream temperature difference and the two pressure drops on either side of the heat transfer surface. As the heat exchanger entropy generation decreases, the pressure drop across the turbine increases, resembling more closely the pressure rise provided by the compressor. Consequently, the turbine power output increases. At the same time, the inlet temperature to the combustion chamber (heater) increases, hence, the specific fuel consumption decreases. We see that the reduction in entropy generation in the counterflow heat exchanger (reduction indicated by $N_{S,a} < 1$) can be measured directly as an increase in energy conversion efficiency.

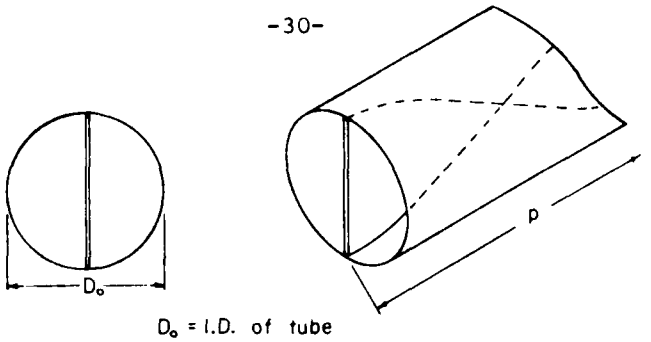

D_o = I.D. of tube
p = pitch (180°)

a

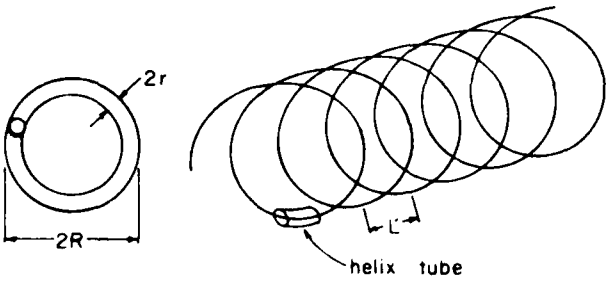

2r = I.D. of tube
2R = diameter of helix
L = coil spacing

b

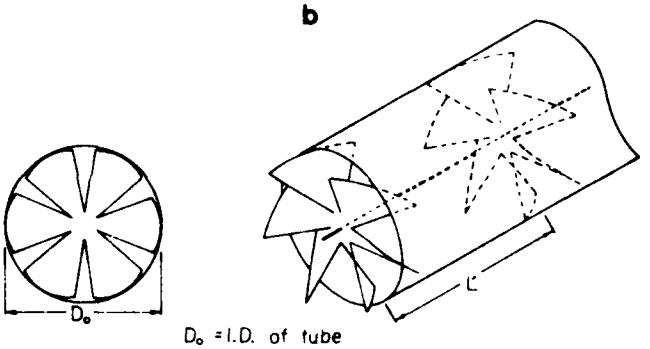

D_o = I.D. of tube
L = propeller spacing

c

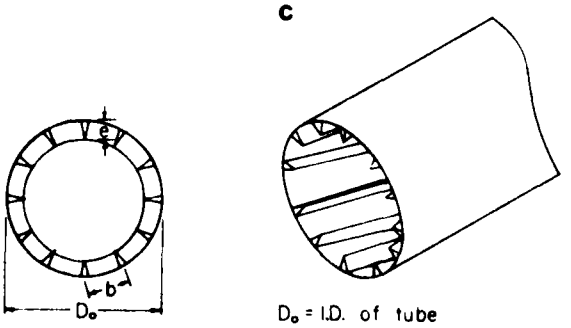

D_o = I.D. of tube
b = interfin spacing
e = fin height

d

Fig. 3.1. Schematic of four swirl flow-promoting techniques for heat-transfer augmentation.

respectively. Equation (3.4) shows that, when the reference passage is dominated by heat transfer irreversibility ($\phi_o \to 0$), the augmentation number $N_{S,a}$ reduces to N_T which is proportional to the ratio of heat transfer coefficients (reference/augmented). In general, however, the augmentation entropy generation number $N_{S,a}$ is a function of the ratio of heat transfer coefficients and the friction factor ratio.

In what follows, we use Eq.s (3.4)-(3.6) to evaluate the relative change in irreversibility introduced by each of the augmentation techniques of Fig. 3.1. We obtain this result by using published heat transfer (St) and fluid friction (f) information on each of these flow geometries.

3.2 Twisted Tape Inserts

The use of twisted tape inserts to augment both laminar and turbulent convective heat transfer is one of the most common in-tube augmentation techniques. This technique is also well-documented. For example, Lopina and Bergles [3.2] measured the heat transfer and fluid-friction characteristics of a tightly inserted uninsulated tape in turbulent flow. The tape was inserted in a straight tube and the assembly was redrawn, with tape in place. This operation forced the tape to slightly penetrate the interior surface of the tube. The geometry of the augmented arrangement is shown schematically in Fig. 3.1(a). The experimental results for St_a and f_a agree to within 10% with the published work of other experimenters.

Figure 3.2 illustrates the augmentation entropy generation number for twisted tape inserts in turbulent flow, based on the data of Lopina and Bergles [3.2]. On this basis, we obtain

$$y = 2.45, \quad N_T = 0.49/(1 + 0.89\ Re_o^{-0.13}) \ , \quad N_P = 2.33 \ ; \qquad (3.8)$$

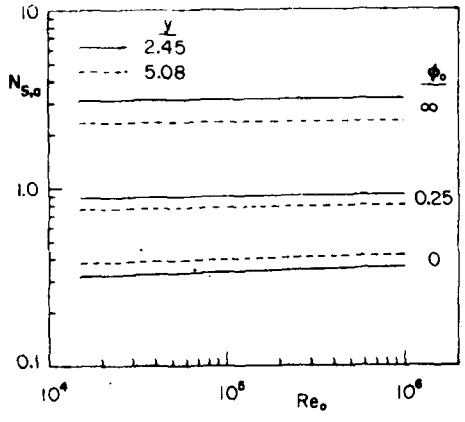

Fig. 3.2. Augmentation entropy generation number for twisted tape inserts.

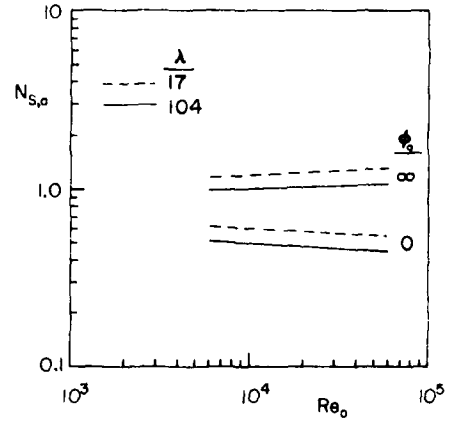

Fig. 3.3. Augmentation entropy generation number for helix-shaped tubes.

$$y = 5.08 \ , \quad N_T = 0.44/(1 + 1.3\ Re_o^{-0.13}) \ , \quad N_P = 3.13 \ ; \qquad (3.9)$$

also

$$D_a/D_o = 0.61 \ , \quad A_a/A_o \simeq 1 \ .$$

In this example, the geometry of Fig. 3.1(a) is the augmented design, vis-a-vis the smooth straight tube which is used as reference.

It is evident from Fig. 3.2 that the parameter which influences $N_{S,a}$ the most is the irreversibility distribution ratio ϕ_o. Thus, whenever ϕ_o is less than approx. 0.25, the use of twisted tape inserts will lead to a reduction in thermodynamic irreversibility. The greatest reduction occurs when $\phi_o = 0$, i.e., when the fluid friction contribution to S' is totally negligible and $N_{S,a}$ becomes proportional to the ratio of heat transfer coefficients, [see Eq. (3.5)]. It is important to note that the critical value of ϕ_o above which the augmentation technique will actually increase the rate of entropy generation, $\phi_o \simeq 0.25$, corresponds to a heat exchanger passage in which the fluid friction contribution amounts to only 20% of S'. Therefore, even in cases clearly dominated by heat transfer irreversibility ($\phi_o < 1$) it is important to evaluate the total entropy generation rate and the change induced in it by the implementation of a proposed augmentation technique, before deciding whether heat transfer augmentation is thermodynamically advantageous.

Figure 3.2 shows also that other parameters, such as Re_o and y, are not nearly as important in affecting the value of $N_{S,a}$. In particular, the augmentation entropy generation number is almost independent of the reference Reynolds number, Re_o. This behaviour follows from the fact that the measured Re_a dependence of St_a and f_a if functionally the same as that of St_o and f_o (see Refs. [3.2] and [3.3]).

The twist ratio y has a visible effect on the entropy generation rate; for example, when ϕ_o approaches zero a tighter twist ($y = 2.45$) is preferable. On the other hand, for values of ϕ_o other than in the $\phi_o \to 0$ limit, i.e., when the fluid friction irreversibility begins to play a role, a looser twist is more advantageous ($y = 5.08$). In fact, using a more extensive collection of experimental data, it may be possible to determine the required twist ratio y which, for a given ϕ_o, is capable of lowering $N_{S,a}$ below a predetermined value.

3.3 Helical Tubes

Another heat transfer augmentation feature common in advanced heat exchanger design is the use of spiraled tubes. In this configuration the swirl flow induced in the stream filling the tube is the result of centrifugal forces. As shown in Fig. 3.1(b), the geometry is described by the ratio $\lambda = R/r$.

Figure 3.3 was constructed by using the heat-transfer and fluid-friction measurements reported by Seban and McLaughlin [3.4],

$$N_T = (\lambda^2/Re_o)^{0.05}, \quad N_P = (Re_o/\lambda^2)^{0.05}, \quad D_a/D_o = 1, \quad A_a/A_o = 1. \tag{3.10}$$

In Fig. 3.3, we show the augmentation entropy generation number in turbulent flow for only two geometries, $\lambda = 17$ and $\lambda = 104$. For brevity, the analysis leading from the Seban and McLaughlin correlations [3.4] to Eq. (3.10) is not shown. However, the reader can find an outline of this analysis in Ref. [3.3].

The chief conclusion to be drawn from Fig. 3.3 is that shaping the tube as a helix has only a minor effect on the rate of entropy generation in the tube. In the limit $\phi_o \to 0$, the irreversibility is reduced to roughly 50% of

the original (reference) value. In the opposite extreme, when fluid friction dominates, ($\phi_o \to \infty$), entropy generation number is of order one. This means that the coiling of the tube has little effect on the overall pressure drop across the tube. Consequently, for a wide range of values of ϕ_o the use of helical tubes leads to a reduction in entropy generation.

3.4 Propeller Inserts

A swirl flow promoting technique similar to twisted tape inserts is shown schematically in Fig. 3.1(c). This augmentation technique consists of a sequence of propellers placed rigidly inside a circular duct.

In this section we evaluate the augmentation entropy generation number corresponding to the air experiments reported by Koch [3.5]. The propeller-shaped inserts investigated by Koch were fabricated by making six radial cuts (almost to the center) in a 50 mm diameter disc. The resulting blades were twisted to approx. a 45° angle. A brass rod was then inserted through the center of each disc and the rod and discs assembly was soldered, maintaining a disc-to-disc spacing L'. The solid assembly was then inserted in a straight tube and secured in place to prevent rotation.

Using Koch's data [3.5] we derive the following extreme values of the augmentation entropy generation number, N_T and N_P:

$$L' = 49 \text{ mm}, \; N_T = 0.035 \; Re_o^{0.15}, \; (L'/D_o = 1) N_P = 59.8 \; Re_o^{-0.009}, \; D_a/D_o = 0.66 \tag{3.11}$$

$$L' = 98 \text{ mm}, \; N_T = 0.078 \; Re_o^{0.114}, \; (L'/D_o = 2) N_P = 32.4 \; Re_o^{-0.011}, \; D_a/D_o = 0.80; \tag{3.12}$$

$$L' = 325 \text{ mm}, \; N_T = 0.153 \; Re_o^{0.085}, \; (L'/D_o = 6.5) N_P = 8.6 \; Re_o^{0.094}, \; D_a/D_o = 0.93; \tag{3.13}$$

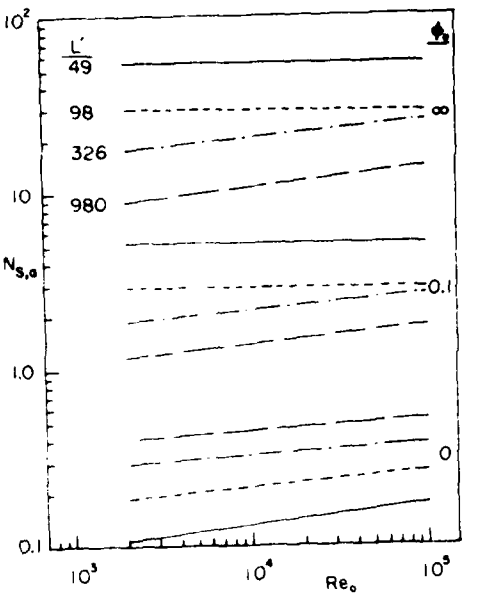

Fig. 3.4. Augmentation entropy generation number for propeller-shaped inserts.

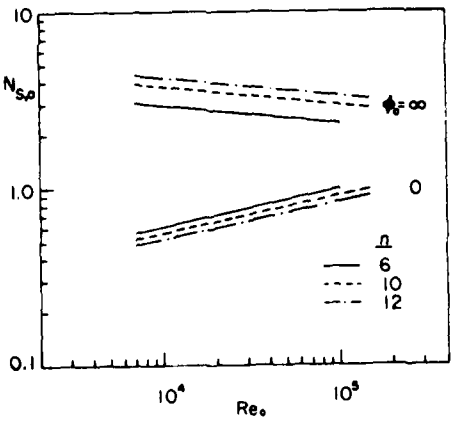

Fig. 3.5. Augmentation entropy generation number for internal straight fins.

$$L' = 980 \text{ mm}, \quad N_T = 0.21\ Re_o^{0.085}, \quad (L'/D_o = 19.6)N_P = 3.83\ Re_o^{0.11}, \quad D_a/D_o = 0.98; \tag{3.14}$$

where $A_a \simeq A_o$.

Figure 3.4 shows the augmentation entropy generation number for three values of irreversibility distribution ratio, $\phi_o = 0, 1, \infty$. As in the preceding examples, the dependence of $N_{S,a}$ on Re_o is weak. However, the maximum reduction in entropy generation is more substantial than in the first two examples. For a relatively dense sequence of propellers, $L' = 49$ mm, in the limit $\phi_o \to 0$ the entropy generation rate is reduced by as much as a factor of ten. Figure 3.4 also shows that, depending on L', the reference irreversibility distribution ratio ϕ_o must be less than 0.05 if propeller inserts are to be effective in conserving available work.

3.5 Internally Finned Tubes

Figure 3.1(d) shows schematically a round tube covered internally with straight or spiraled fins. This augmented tube geometry has been studied extensively. For example, Bergles et al. [3.6] and Carnavos [3.7] have measured the heat transfer and fluid friction characteristics of approximately thirty straight and spiraled internally finned geometries. Empirical formulae generated by Carnavos [3.7] correlate within 10% the bulk of the existing experimental information.

In this section, we use the Carnavos correlations to examine the relationship between internal finning and entropy generation. A first objective is to determine the difference between straight and spiraled fins of otherwise similar geometry. The effect of fin density and twist ratio is also illustrated.

Figure 3.5 shows the change in entropy generation rate due to straight internal fins in turbulent flow, for the two extremes $\phi_o = 0, \infty$. Three different geometries

have been considered, n = 6, 10, 12, where n is the number of fins. The results of the entropy generation analysis which led to Fig. 3.5 can be summarized as follows [3.3]:

$$\text{for } n = 6\,,\ N_T = 0.097\ Re_o^{0.2}\,,\ N_P = 7.35\ Re_o^{-0.1}\,,\ D_a/D_o = 0.74\,,\ A_a/A_o = 0.94\,; \tag{3.15}$$

$$\text{for } n = 10\,,\ N_T = 0.089\ Re_o^{0.2}\,,\ N_P = 9.45\ Re_o^{-0.1}\,,\ D_a/D_o = 0.61\,,\ A_a/A_o = 0.91\,; \tag{3.16}$$

$$\text{for } n = 12,\ N_T = 0.084\ Re_o^{0.2}\,,\ N_P = 10.6\ Re_o^{-0.1}\,,\ D_a/D_o = 0.57\,,\ A_a/A_o = 0.89\,. \tag{3.17}$$

It is evident that, almost independently of n, the reduction in entropy generation is small even in the limit $\phi_o \to 0$, particularly as the Reynolds number increases. The change in entropy generation rate is more pronounced as the number of fins increases.

Greater reductions in entropy generation are achieved when the internal fins are twisted, thereby inducing a swirl motion in the core of the tube cross section. In Fig. 3.6, we show the augmentation entropy generation number corresponding to a finned tube with $n = 10$ and the values of twist ratio, $y = 5.62$ and $y = 9.27$. In general, the augmentation entropy generation number is given by Eq. (3.4) combined with

$$N_T = 0.052\ Re_o^{0.17} y^{0.27}\,,\ N_P = 15.2\ Re_o^{-0.13} y^{-0.2}\,,\ D_a/D_o = 0.61\,,\ A_a/A_o = 0.91\,. \tag{3.18}$$

Provided the irreversibility distribution ratio ϕ_o is small enough, the reduction in entropy generation rate increases as y decreases, i.e., as the fin twist

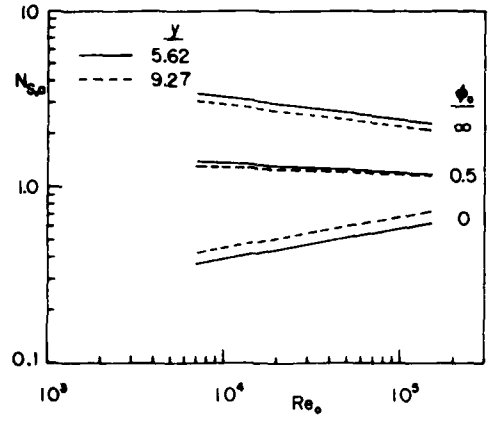

Fig. 3.6. Augmentation entropy generation number for internal spiraled fins.

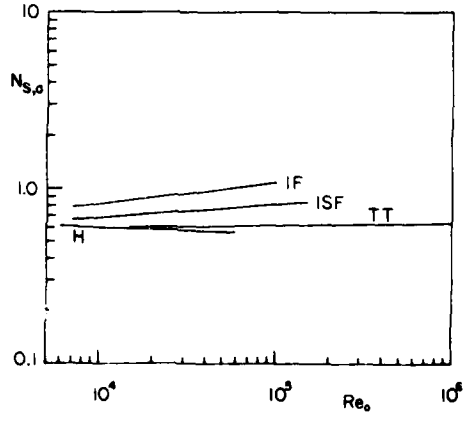

Fig. 3.7. Comparison of four swirl promoters based on irreversibility minimization potential in a ϕ_o=0.1 application; IF=internal straight fins (n=10); ISF=internal spiraled fins (n=10,y=9.27); TT=twisted tape (y=5.08); H=helical tube (λ=30).

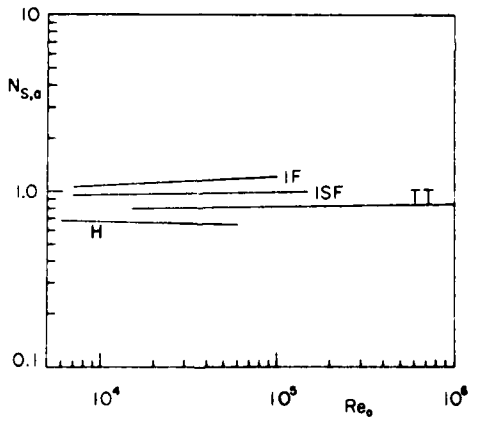

Fig. 3.8. Comparison of four swirl promoters based on irreversibility minimization potential in a ϕ_o=0.25 application; IF=internal straight fins (n=10); ISF=internal spiraled fins (n=10, y=9.27); TT=twisted tape (y=5.08); H=helical tube (λ=30).

becomes tighter. This conclusion is qualitatively similar to the one encountered earlier in the analysis of twisted tape inserts.

Comparing the curves of Fig. 3.6 with the $n = 10$ curves of Fig. 3.5, we conclude that the twist of internal fins can have a significant effect on the available work conservation potential of the finning technique. For example, in the limit $\phi_o \to 0$, the spiraled fin irreversibility is about 50% less than in the case of straight fins.

An important observation is that the spiraled fins entropy-generation number $N_{S,a}(\phi_o, Re_o, y)$, given by Eqs. (3.4) and (3.18), is not a monotonic function of twist ratio y. In fact, when the heat exchanger passage is specified (i.e., ϕ_o and Re_o are fixed), one can determine the optimum twist ratio y_{opt} yielding the largest reduction in entropy generation rate (minimum $N_{S,a}$). Setting $\partial N_{S,a}/\partial y = 0$ and $\partial N_{S,a}/\partial y > 0$, we obtain

$$y_{opt} = 9.4 \times 10^4 \, \phi_o^{2.13} \, Re_o^{-0.64} . \qquad (3.19)$$

For example, in an application in which $\phi_o = 0.2$ and $Re_o = 10^4$, the optimum twist ratio is $y_{opt} = 8.4$, yielding the minimum $N_{S,a}^{min} = 0.868$. If, in the same application, heat transfer is augmented using fins with twist ratios $y \neq y_{opt}$, say $y = 5$ or $y = 15$, the entropy generation reduction is inferior and $N_{S,a} = 0.875$ and $N_{S,a} = 0.876$, respectively.

3.6 Internally Roughened Tubes

Finally, we illustrate the evaluation procedure in the case of "in-tube roughness) which is one of the most common and amply documented heat transfer augmentation techniques. In this case the augmentation entropy generation number (3.4) assumes the simpler form

$$N_{S,a} = \frac{St_o}{St_a} + \frac{\phi_o}{1 + \phi_o} \left(\frac{f_a}{f_o} - \frac{St_o}{St_a} \right) \qquad (3.20)$$

since, in almost all rough-tube designs, $D_a \simeq D_o$ and $A_a \simeq A_o$. Consequently, the Reynolds number in the augmented (rough) tube is equal to the Reynolds number in the reference (smooth) tube. The entropy generation number for in-tube roughness emerges as a weighted function of the Stanton number ratio and the friction factor ratio. The two ratios are weighted according to the irreversibility distribution parameter ϕ_o, in other words, with respect to the irreversible mode of operation of the heat exchanger duct (fluid friction vs. heat transfer).

Figure 3.9 shows the entropy generation number as a function of Re_o and ϕ_o. The figure was constructed for $Pr = 0.72$ using the data of Refs. [3.8,3.9] for sand grain (f_a, St_a) and the correlation of Refs. [3.10,3.11] for smooth tubes (f_o, St_o). It is evident that the ability of sand-grain roughened walls to reduce irreversibility depends on ϕ_o and Re_o. The effect of roughness height e/D on entropy generation increases steadily as the Reynolds number increases. As one might expect, the change in $N_{S,a}$ is more pronounced in the case of larger e/D.

From an engineering standpoint, it is important to know under what conditions the wall-roughening leads to a reduction in entropy generation. In Fig. 3.10 we plotted the marginal curves $\phi_o(Re_o)$ resulting from setting $N_{S,a} = 1$ in equation (3.20). Below each curve, roughening the wall will decrease the irreversibility rate. Above each curve, wall-roughening will increase the rate of entropy generation.

Figures 3.11-3.14 show the augmentation entropy generation number $N_{S,a}$ and marginal curves $\phi_o(Re_o)$ for repeated ribs of the type sketched in the insert of Fig. 3.11. This geometry is characterized by two aspect ratios, the rib

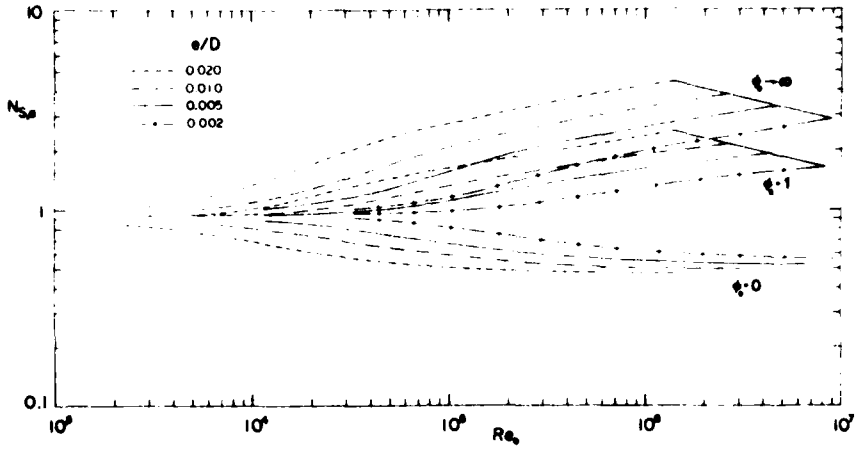

Fig. 3.9. Augmentation entropy generation number for sand-grain roughness.

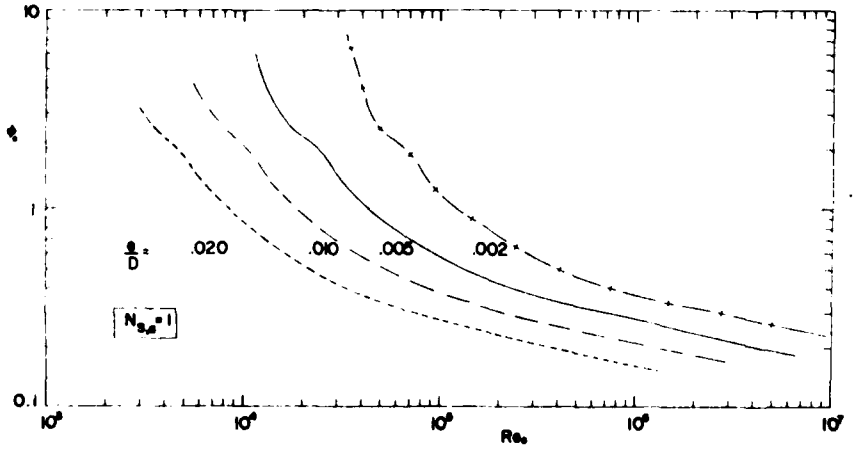

Fig. 3.10. Critical irreversibility distribution ratio ϕ_o for sand-grain roughness.

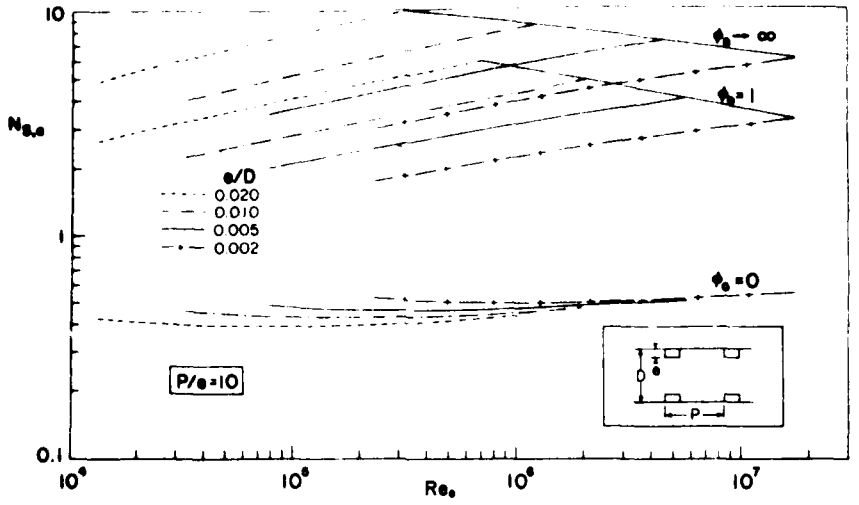

Fig. 3.11. Augmentation entropy generation number for repeated rib roughness; effect of rib height e/D .

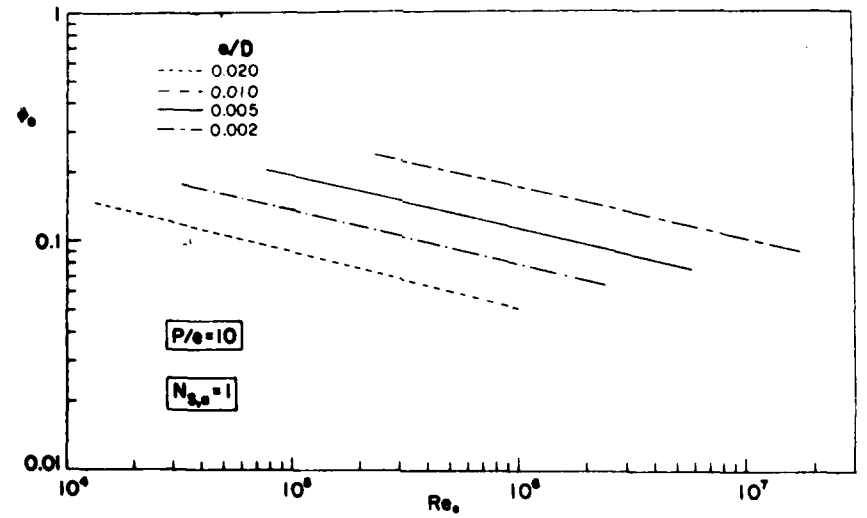

Fig. 3.12. Critical irreversibility distribution ratio ϕ_o for repeated rib roughness; effect of rib height e/D .

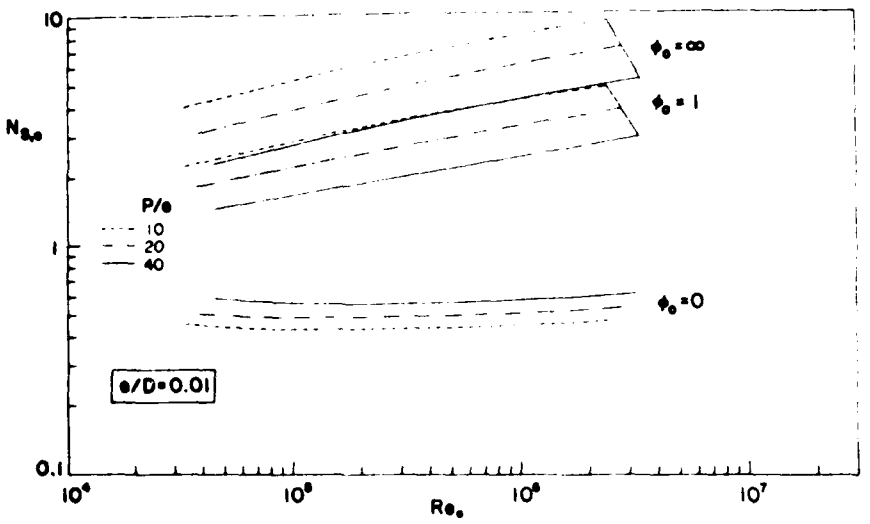

Fig. 3.13. Augmentation entropy generation number for repeated rib roughness; effect of rib spacing P/e .

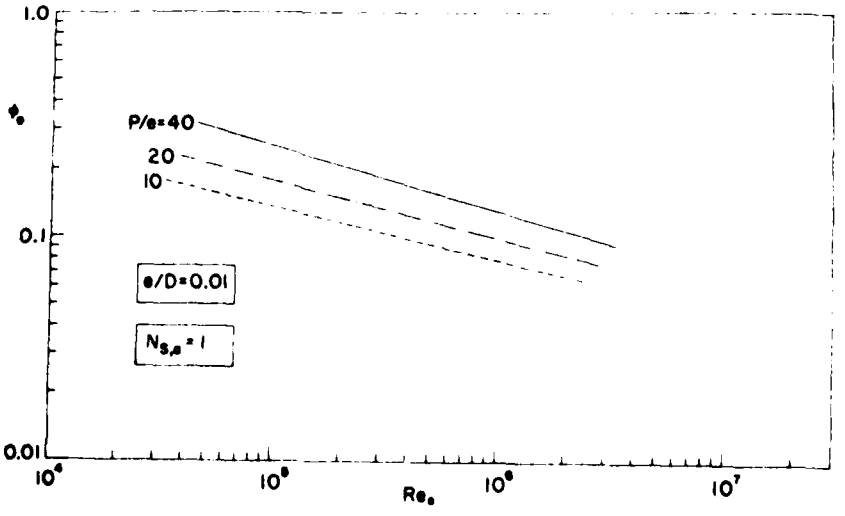

Fig. 3.14. Critical irreversibility distribution ratio ϕ_o for repeated rib roughness; effect of rib spacing P/e .

height e/D and the rib spacing P/e. The graphs were constructed for $Pr = 0.72$ using the friction factor and Stanton number correlations of Webb, et al. [3.12]. There are obvious similarities between these plots and Figs. 3.9 and 3.10 for sand-grain roughness. The more significant difference is that, with Re_o and e/D fixed, Figs. 3.12 and 3.14 yield marginal irreversibility distribution ratios ϕ_o about four times less than Fig. 3.10. In other words, repeated ribs of a given height $(e/D)_1$ correspond to sand-grain roughness with grain height significantly greater than $(e/D)_1$.

The effect of rib spacing (P/e) is summarized in Figs. 3.13, 3.14. We find that the rib spacing has a relatively weaker effect on entropy generation than the rib height (Figs. 3.11, 3.12). Furthermore, the change induced in the entropy generation number decreases steadily as the rib spacing increases. This trend is in agreement with the effect of decreasing e/D for sand grain (Fig. 3.9); increasing the rib spacing while keeping the rib height constant is equivalent to gradually smoothing out the tube surface.

An important observation concerns the minima in the $N_{S,a}$ curves, Figs. 3.11, 3.13, particularly in the ϕ_o range in which the use of repeated ribs leads to a reduction in irreversibility. For a given heat exchanger duct (ϕ_o, Re_o) it is possible to determine a priori the optimum rib geometry which yields the maximum reduction in the rate of entropy generation. For example, in Fig. 3.15 we report the optimum rib height $(e/D)_{opt}$ for cases where the relative spacing is fixed, $P/e = 10$. Note that the irreversibility distribution ratio ϕ_o has a marked effect on the optimum rib height for minimum $N_{S,a}$, despite the fact that numerically ϕ_o is very small.

3.7 Other heat transfer augmentation techniques

In this chapter we reviewed the impact of heat transfer augmentation on entropy generation in the case of a limited number of augmentation techniques.

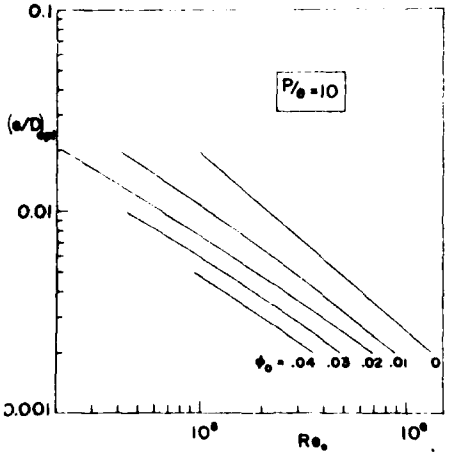

Fig. 3.15. Optimum rib height for minimum exergy destruction.

For a considerably more complete study the reader should consult the thesis by Ouellette [3.3]. In addition to the techniques highlighted in this chapter, Ouellette's thesis analyzes the entropy generation due to

I - extended surfaces
- internal fins
- mesh inserts

II - roughened surfaces
- thread-type roughness
- screen roughness
- wire-wound roughness

III - displaced enhancement devices
- suspended discs
- suspended rings

IV - compound techniques
- twisted tape with fin effect
- internally spiraled fins

The analytical results of Ouellette's study are summarized here in Tables 3.1-3.5.

TABLE 3.1

SUMMARY OF PROPELLER INSERTS AND TWISTED TAPE

Technique	Configuration	Fluid	Low/Turbulent Re_o Range	Tube or Parameter		$\frac{D_a}{D_o}$	$\frac{Re_a}{Re_o}$	N_P	N_T
Propeller Inserts	Tubular	Air	Turbulent $2x10^3$ - $1x10^5$	Distance between inserts L'(mm)	L' = 49	0.66	0.66	$59.8\ Re_o^{-0.259}$	$0.0345\ Re_o^{0.149}$
					L' = 98	0.80	0.80	$32.4\ Re_o^{-0.011}$	$0.776\ Re_o^{0.114}$
					L' = 326	0.93	0.93	$3.59\ Re_o^{+0.094}$	$0.153\ Re_o^{0.085}$
					L' = 980	0.98	0.98	$3.89\ Re_o^{+0.116}$	$0.208\ Re_o^{0.085}$
Twisted Tape	Tubular	H_2O	Laminar 35 - 1500	Twist ratio	y = 2.45	0.61	0.61	7.71	$5.45\ Re_o^{-0.622}$
					y = 5.08			7.71	$8.58\ Re_o^{-0.622}$
			Turbulent 10^4 - 10^6		y = 2.45	0.61	0.61	3.13	$0.0204\ Re_o^{0.8}$ / $0.0422\ Re_o^{0.8} + 0.0547\ Re_o^{0.67}$
					y = 5.08			2.33	$0.0204\ Re_o^{0.8}$ / $0.0381\ Re_o^{0.8} + 0.0337\ Re_o^{0.67}$

TABLE 3.2

SUMMARY OF HELIX

Technique	Configuration	Fluid	Low/Turbulent Re_o Range	Tube or Parameter		$\frac{D_a}{D_o}$	$\frac{Re_a}{Re_o}$	N_P	N_T
Helix	Tubular	H_2O	Laminar	Aspect	$\lambda = 3$	1.0	1.0	$1.0 + 3.493 \times 10^{-3} Re_o - 2.096 \times 10^{-7} Re_o^2$	$\frac{4.364}{1.064 + 0.691 Re_o^{0.5}}$
			$10^2 - 10^3$	ratio	$\lambda = 10$			$1.0 + 1.624 \times 10^{-3} Re_o - 2.096 \times 10^{-7} Re_o^2$	$\frac{4.364}{1.064 + 0.512 Re_o^{0.5}}$
				$\lambda \equiv R/r$	$\lambda = 3$			$1.0 + 1.093 \times 10^{-3} Re_o - 2.096 \times 10^{-7} Re_o^2$	$\frac{4.364}{1.064 + 0.389 Re_o^{0.5}}$
			Turbulent		$\lambda = 3$			$0.896\ Re_o^{0.05}$	$1.12\ Re_o^{-0.05}$
			$6 \times 10^2 - 6.5 \times 10^4$		$\lambda = 10$			$0.794\ Re_o^{0.05}$	$0.993\ Re_o^{-0.05}$
					$\lambda = 30$			$0.712\ Re_o^{0.05}$	$0.890\ Re_o^{-0.05}$

TABLE 3.3

SUMMARY OF INTERNAL FINS, MESH INSERTS AND SCREEN ROUGHNESS

Technique	Configuration	Fluid	Low/Turbulent Re_o Range	Tube or Parameter		$\frac{D_a}{D_o}$	$\frac{Re_a}{Re_o}$	N_f	N_T
Internal fins	Tubular	H_2O	Turbulent 7×10^3 - 1.5×10^5	Number of fins n	n = 6	0.74	0.78	$7.15\ Re_o^{-0.14}$	$0.0966\ Re_o^{0.20}$
					n = 10	0.61	0.68	$9.45\ Re_o^{-0.14}$	$0.887\ Re_o^{0.20}$
					n = 12	0.57	0.64	$10.6\ Re_o^{-0.14}$	$0.837\ Re_o^{0.20}$
Mesh inserts	Tubular	H_2O	Turbulent 8×10^3 - 3.2×10^5	Tube number	No. 13	7×10^{-1}	8.7×10^{-2}	$34.9\ Re_o^{-0.345}$	$8.01 \times 10^{-5}\ Re_o^{0.290}$
					No. 14			$46.6\ Re_o^{-0.132}$	$4.38 \times 10^{-4}\ Re_o^{0.041}$
					No. 15			$221.0\ Re_o^{-0.239}$	$3.38 \times 10^{-3}\ Re_o^{-0.20}$
Screen Roughness	Annular	Air	Turbulent 4×10^4 - 2×10^5	Mesh size	10 x 10	1.0	1.0	$2.80\ Re_o^{-0.032}$	$0.843\ Re_o^{-0.052}$
					20 x 20			$2.57\ Re_o^{-0.026}$	$1.085\ Re_o^{-0.072}$
					30 x 30			$5.37\ Re_o^{-0.113}$	$3.41\ Re_o^{-0.59}$

TABLE 3.4

SUMMARY OF THREAD TYPE ROUGHNESS AND WIRE WOUND ROUGHNESS

Technique	Configuration	Fluid	Low/Turbulent Re_o Range	Tube or Parameter		$\frac{D_a}{D_o}$	$\frac{Re_a}{Re_o}$	N_P	N_T
Thread type roughness	Tubular	Air	Turbulent $10^5 - 10^6$	Threads per inch	11 t.p.i.	0.5	0.5	$0.576\ Re_o^{0.2}$	$0.666\ Re_o^{-0.07}$
					24 t.p.i.			$0.452\ Re_o^{0.2}$	$0.968\ Re_o^{-0.09}$
					60 t.p.i.			$0.308\ Re_o^{0.2}$	$2.60\ Re_o^{-0.15}$
	Annular	Air	Turbulent $10^5 - 5 \times 10^5$		11 t.p.i.	0.6	0.6	$0.298\ Re_o^{0.282}$	$0.523\ Re_o^{-0.028}$
					24 t.p.i.			$0.180\ Re_o^{0.282}$	$1.90\ Re_o^{-0.110}$
					60 t.p.i.			$0.130\ Re_o^{0.282}$	$7.35\ Re_o^{-0.209}$
			Turbulent $10^5 - 6 \times 10^5$		24 rough/rough	0.5	0.5	$1.54\ Re_o^{0.152}$	$0.279\ Re_o^{-0.010}$
Wire Wound Roughness	Annular	Air	Turbulent $6 \times 10^4 - 2 \times 10^5$	Number of wire starts n p/c=8	n = 1	1.0	1.0	$0.716\ Re_o^{0.194}$	$0.811\ Re_o^{0.048}$
					n = 4			$0.737\ Re_o^{0.194}$	$0.800\ Re_o^{-0.048}$
					n = 10			$0.379\ Re_o^{0.232}$	$1.029\ Re_o^{-0.060}$
					n = 16			$0.937\ Re_o^{0.132}$	$1.44\ Re_o^{-0.088}$
				Number of wire starts n p/c=16	n = 1			$0.589\ Re_o^{0.199}$	$1.11\ Re_o^{-0.060}$
					n = 4			$0.526\ Re_o^{0.199}$	$1.15\ Re_o^{-0.060}$
					n = 6			$0.368\ Re_o^{0.215}$	$1.23\ Re_o^{-0.060}$
					n = 16			$0.674\ Re_o^{0.115}$	$1.69\ Re_o^{-0.078}$

TABLE 3.5

SUMMARY OF SUSPENDED RINGS, SUSPENDED DISCS, TWISTED TAPE WITH FIN EFFECT AND INTERNALLY SPIRALED FINS

Technique	Configuration	Fluid	Low/Turbulent Re_o Range	Tube or Parameter		$\frac{D_a}{D_o}$	$\frac{Re_a}{Re_o}$	N_P	N_T
Suspended Rings	Tubular	Air	Turbulent $2 \times 10^3 - 1 \times 10^5$	Ring thickness K(mm)	K = 3.75	0.85	0.85	$2.18\ Re_o^{-0.244}$	$0.213\ Re_o^{-0.047}$
					K = 2.25			$1.44\ Re_o^{-0.236}$	$0.164\ Re_o^{-0.089}$
Suspended Discs	Tubular	Air	Turbulent $2 \times 10^3 - 1 \times 10^5$	Tube designator (see Table I)	A	0.89	0.89	$1.56\ Re_o^{-0.24}$	$0.324\ Re_o^{-0.034}$
					B	0.95	0.95	$1.02\ Re_o^{-0.23}$	$0.519\ Re_o^{-0.012}$
					E	0.84	0.84	$4.12\ Re_o^{-0.26}$	$0.182\ Re_o^{-0.035}$
					F	0.91	0.91	$2.72\ Re_o^{-0.26}$	$0.201\ Re_o^{-0.054}$
					H	0.79	0.79	$78.2\ Re_o^{-0.148}$	$0.137\ Re_o^{-0.006}$
					I	0.90	0.90	$16.9\ Re_o^{-0.23}$	$0.223\ Re_o^{-0.001}$
Twisted Tape with fin effect	Tubular	H_2O	Turbulent $1.5 \times 10^4 - 1.5 \times 10^6$	Twist ratio y	y = 2.45	0.61	0.61	3.13	$\frac{0.0185\ Re_o^{-0.8}}{0.0422\ Re_o^{-0.8} + 0.0547\ Re_o^{-0.67}}$
					y = 5.08			2.33	$\frac{0.0185\ Re_o^{-0.8}}{0.0381\ Re_o^{-0.8} + 0.0337\ Re_o^{-0.67}}$
Internally Spiraled fns	Tubular	H_2O	Turbulent $7 \times 10^3 - 1.5 \times 10^5$	Twist ratio y	y = 5.62	0.61	0.68	$10.8\ Re_o^{-0.13}$	$0.0830\ Re_o^{-0.17}$
					y = 9.27			$9.74\ Re_o^{-0.13}$	$0.0950\ Re_o^{-0.17}$

References

3.1 A. Bejan, Int. J. Heat Mass Transfer 21, 655 (1978).

3.2 R.F. Lopina and A.E. Bergles, J. Heat Transfer, Trans, ASME 91, 434 (1969).

3.3 W.R. Ouellette, "Entropy Generation Criterion Applied to Various Heat Transfer Augmentation Techniques," M.S. Thesis, Department of Mechanical Engineering, University of Colorado, Boulder (Aug. 1979); copies available on request.

3.4 R.A. Seban and E.F. McLaughlin, Int. J. Heat Mass Transfer 6, 387 (1963).

3.5 R. Koch, VDI - Forschungsheft 24B, 1 (1958).

3.6 A.E. Bergles, G.S. Brown, Jr., and W.D. Snider, "Heat Transfer Performance of Internally Finned Tubes," ASME Paper 71-HT-31, 1971.

3.7 T.C. Carnavos, "Some Recent Developments in Augmented Heat Exchange Elements," Heat Exchanger Design and Theory Sourcebook (edited by N.H. Afgan and E.U. Schlunder), p. 441. Scripta Book Co., Washington, D.C. (1974).

3.8 J. Nikuradse, NACA TM 1292, November 1950.

3.9 D.F. Dipprey, R.H. Sabersky, Int. J. Heat Mass Transfer 6, 329 (1963).

3.10 W.M. Kays, H.C. Perkins, Handbook of Heat Transfer, W.M. Rohsenow and J.P. Hartnett, editors, McGraw-Hill, New York, 7-4 (1973).

3.11 B.S. Petukhov, Adv. Heat Transfer 6, 503 (1970).

3.12 R.L. Webb, E.R.G. Eckert, R.J. Goldstein, Int. J. Heat Mass Transfer 15, 1647 (1972).

4. EXTENDED SURFACES (FINS) FOR MINIMUM ENTROPY GENERATION

4.1 Entropy generation due to heat transfer from a single fin

The entropy generation associated with a fin in cross-flow can be evaluated based on the general model presented in Fig. 4.1. Consider, then, a solid body of arbitrary shape and surface area A, suspended in a uniform stream of free-stream velocity U_∞ and temperature T_∞. Imagine also a stream tube (control surface) surrounding the solid body, the radius of this tube being considerably larger than the characteristic linear dimension of the body. Since the fluid outside and immediately inside the tube surface belongs to the free stream U_∞, T_∞, the stream tube surface can be regarded as adiabatic and shear-free.

The equations describing the conservation of mass, conservation of energy and generation of entropy in the stream tube are

$$\dot{m}_{IN} = \dot{m}_{OUT} \ , \ \dot{m}h_{IN} + \iint_A q''d\sigma - \dot{m}h_{OUT} = 0 \qquad (4.1,4.2)$$

$$S_{gen} = \dot{m}s_{OUT} - \dot{m}s_{IN} - \iint_A \frac{q''}{T_W}\, d\sigma \ . \qquad (4.3)$$

In these equations q'' and q''/T_W represent the heat flux and entropy flux from the body to the external fluid. Combining equations (4.1)-(4.3) with the canonical equation $dh = T_{ds} + \frac{1}{\rho} dP$, we can express the rate of entropy generation as

$$S_{gen} = \iint_A q'' \left(\frac{1}{T_\infty} - \frac{1}{T_W} \right) d\sigma - \frac{\dot{m}}{\rho\, T_\infty} (P_{OUT} - P_{IN}) \qquad (4.4)$$

Recognizing that $\dot{m} = \rho\, A_\infty\, U_\infty$ and $F_D = A(P_{IN} - P_{OUT})$, the entropy generation

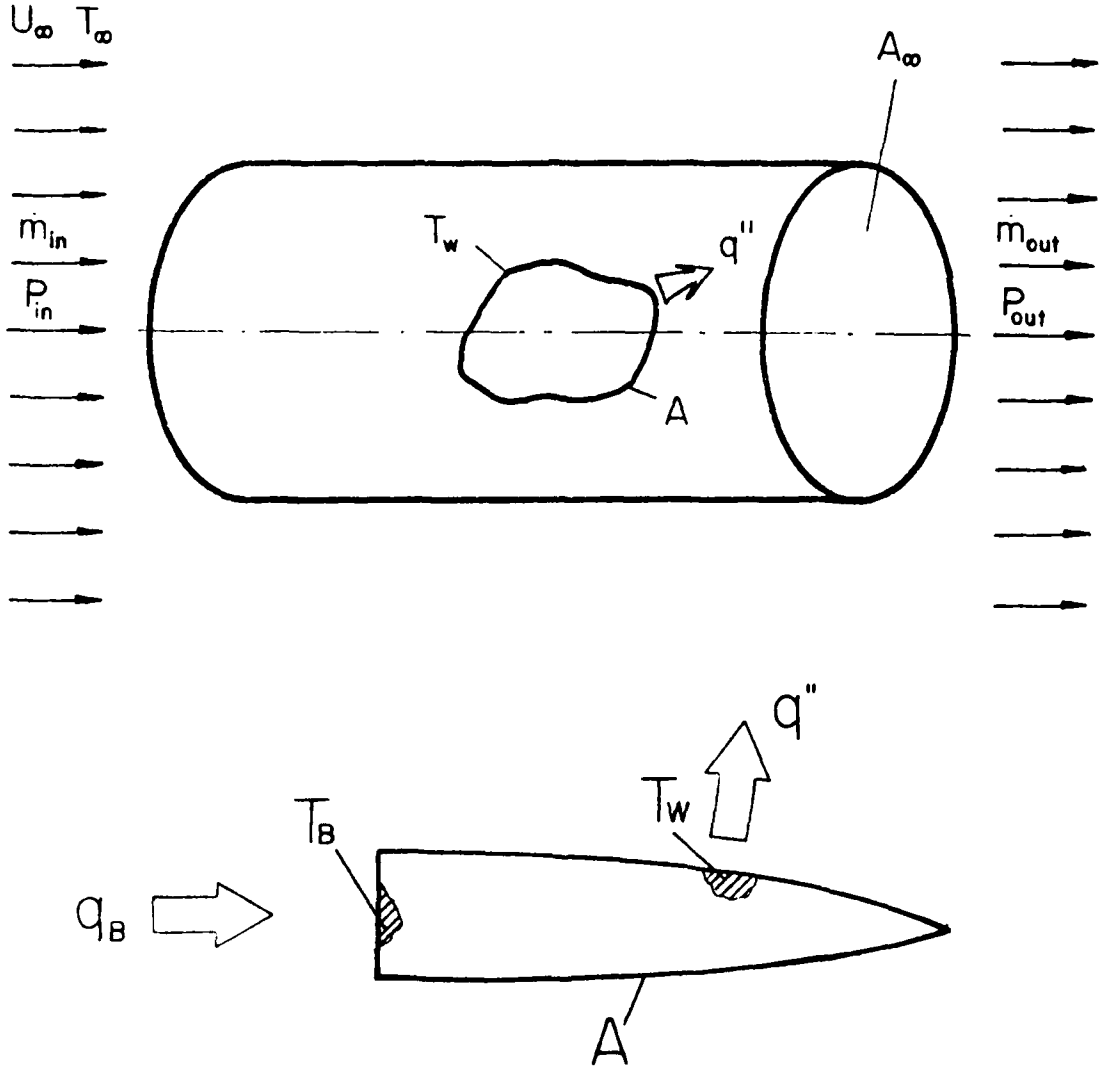

Fig. 4.1. Schematic of a general fin in a convective heat transfer arrangement.

rate can finally be written as

$$S_{gen} = \iint_A q'' \left(\frac{1}{T_\infty} - \frac{1}{T_W} \right) d\sigma + \frac{1}{T_\infty} F_D U_\infty . \tag{4.5}$$

In order to calculate the total rate of entropy generation due to a single fin, it is necessary to recognize that expression (4.5) sums up only the entropy generated in the space surrounding the fin surface. It is easy to see that since the is not an isothermal body, entropy will also be generated internally. In accordance with the second law of thermodynamics applied to the fin shown in the bottom half of Fig. 4.1, the entropy generated inside a single fin is

$$(S_{gen})_{internal} = \iint \frac{q''}{T_W} d\sigma - \frac{q_B}{T_B} \tag{4.6}$$

where q_B and T_B represent the base heat transfer and absolute temperature. The total rate of entropy generation associated with a single fin is obtained by adding equations (4.5) and (4.6) side-by-side,

$$(S_{gen})_{fin} = \frac{q_B \theta_B}{T_\infty^2} + \frac{1}{T_\infty} F_D U_\infty \tag{4.7}$$

In this expression θ_B is the base-stream temperature difference $(T_B - T_\infty)$, which is assumed considerably smaller than the local absolute temperature, T_∞ or T_B.

The fin entropy generation rate, Equation (4.7), is a remarkably simple result which demonstrates that fluid friction and inadequate thermal contact contribute hand-in-hand to the degrading of fin thermodynamic performance. The heat transfer contribution to $(S_{gen})_{fin}$ is proportional to the product of base heat flux times base-fluid temperature difference. Therefore, the

heat transfer entropy generation term can be minimized by reducing θ_B, i.e., by enhancing the base-stream thermal contact. In general, this operation requires an increase in fin size (surface area) which leads automatically to an increase in drag and fluid friction entropy generation. Clearly, the fin size plays an important trade-off role with respect to improving the thermodynamic performance of the individual fin. In what follows we illustrate this trade-off by showing concrete results [4.1] for entropy generation minimization in some of the most common fins encountered in practice.

4.2 Pin Fins

Consider first the pin fin geometry shown in Fig. 4.2(a). This geometry is one of the simplest, because it depends on only two dimensions: the length L and the diameter of the circular cross-section D. According to the unidirectional heat conduction model described in the Introduction, the relationship between base heat flux and base-stream temperature difference is [4.2]

$$\theta_B = \frac{q_B}{\frac{\pi}{4} kD^2 m \tanh(mL)} \; ; \; m = \left(\frac{4\bar{h}}{kD}\right)^{\frac{1}{2}} \; ; \; \bar{h} = \frac{q''}{T_W - T_\infty} \; . \tag{4.8}$$

Substituting this expression into Equation (4.7), the total entropy generation rate can be written as

$$(S_{gen})_{fin} = \frac{q_B^2}{\frac{\pi}{2} T_\infty^2 (\lambda k)^{\frac{1}{2}} Nu^{\frac{1}{2}} Re_D \frac{\nu}{U_\infty} \tanh\left[2Nu^{\frac{1}{2}} \left(\frac{\lambda}{k}\right)^{\frac{1}{2}} \frac{Re_L}{Re_D}\right]} + \frac{\rho \nu^2 U_\infty Re_L Re_D C_D}{2 T_\infty} \tag{4.9}$$

where the drag coefficient is $C_D = F_D/(\frac{1}{2}\rho U_\infty^2 DL)$. Since the external flow is assumed known, we are using the Reynolds number as dimensionless notation

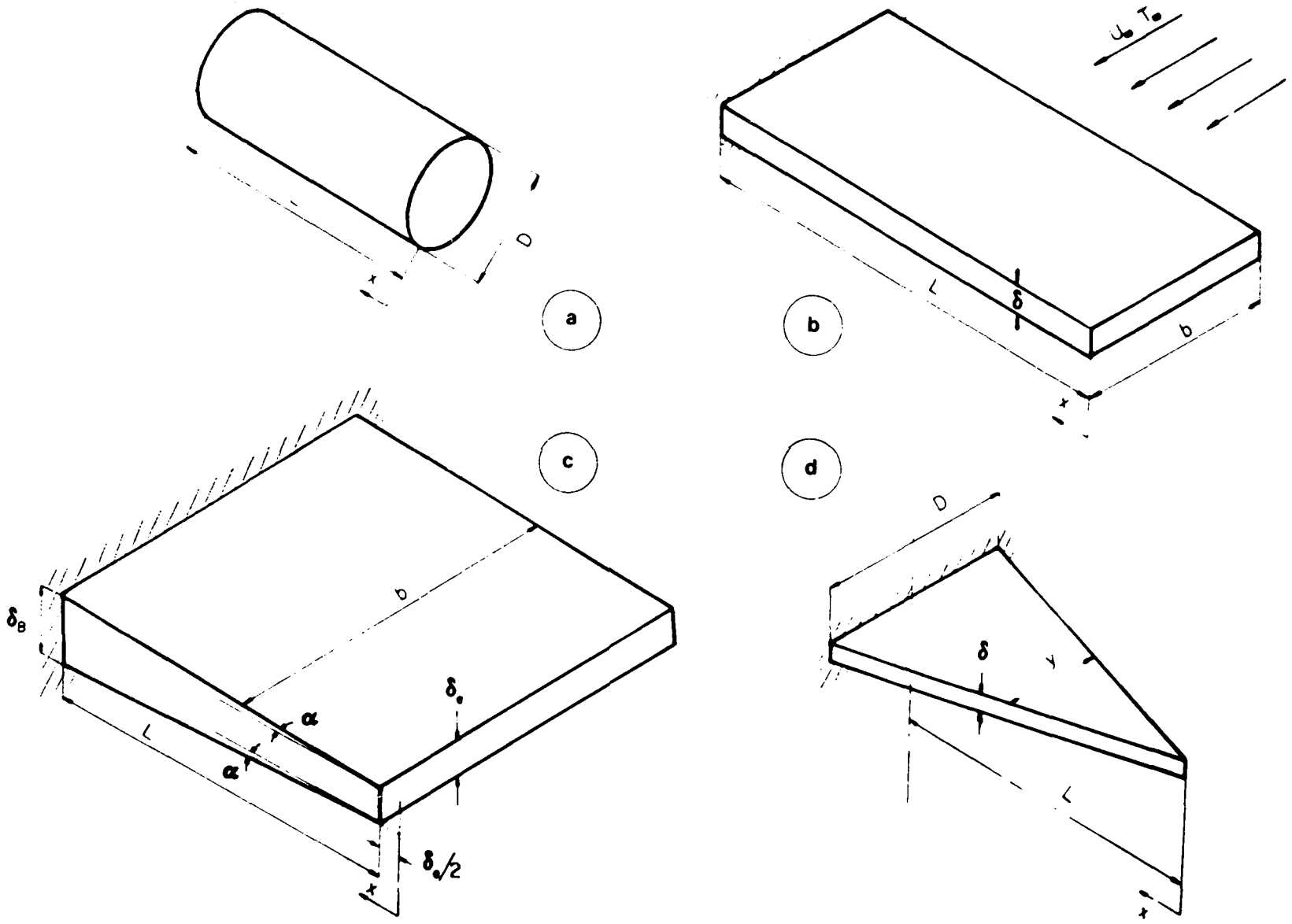

Fig. 4.2. Four common fin geometries: (a) pin fin; (b) rectangular plate fin; (c) rectangular plate fin of trapezoidal profile; (d) triangular plate fin of rectangular profile.

for the two dimensions of the pin fin, $Re_D = U_\infty D/\nu$, $Re_L = U_\infty L/\nu$.

In this study, we adopted the design viewpoint that the "job" of the individual fin is to transfer heat at a known rate (q_B) from the wall to the known stream, in the least irreversible manner possible (with minimum generation of entropy). Therefore, the correct entropy generation number [4.3] for this design problem is constructed as

$$N_S = (S_{gen})_{fin} \Big/ \frac{q_B^{\,2} U_\infty}{k \nu T_\infty^{\,2}}$$

$$= \frac{(k/\lambda)^{1/2}}{\frac{\pi}{2} Nu^{1/2} Re_D \tanh\left[2Nu^{1/2}\left(\frac{\lambda}{k}\right)^{1/2} \frac{Re_L}{Re_D}\right]} + \frac{1}{2} BC_D Re_L Re_D \qquad (4.10)$$

where B is a fixed dimensionless parameter which accounts for the importance of fluid friction irreversibility relative to heat transfer irreversibility,

$$B = \rho \nu^3 k T_\infty / q_B^{\,2} . \qquad (4.11)$$

If the pin fin is slender, the Nusselt number and the drag coefficient can be evaluated from results developed for a single cylinder in cross-flow [4.4]

$$Nu = 0.683 Re_D^{0.466} Pr^{1/3}, \quad C_D = 5.484 Re_D^{-0.246}, \quad 40 < Re_D < 10^3 \qquad (4.12)$$

The entropy generation number N_S emerges as a function of five dimensionless groups, two pertaining to fin geometry (Re_L, Re_D), and three accounting for the working fluid and for the fin-stream convective arrangement (Pr, k/λ, B). Minimization of N_S with respect to Re_L is achieved in a straightforward manner by solving $\partial N_S/\partial Re_L = 0$. The optimum pin length calculated in this manner is

$$Re_{L_{opt}} = \frac{Re_D}{2Nu^{1/2}} \left(\frac{k}{\lambda}\right)^{1/2} \sinh^{-1}\left[\left(\frac{8}{\pi\, Re_D^{3}\, C_D\, B}\right)^{1/2}\right] \tag{4.13}$$

The engineering significance of result (4.13) is that the optimum pin length can be calculated immediately, provided Re_D (hence, Nu and C_D) is specified. In most cases, however, the pin diameter is a design variable which can also be determined on the basis of entropy generation minimization. The optimum diameter for minimum entropy generation $Re_{D_{opt}}$ can be determined by substituting equations (4.12) and (4.13) into equation (4.10), and numerically minimizing N_S.

An alternative approach to sizing a pin fin for minimum irreversibility consists of determining the optimum diameter $Re_{D_{opt}}$ subject to fixed slenderness ratio $\gamma = Re_L/Re_D$. This constraint stems from practical limitations encountered in the process of manufacturing a surface covered with a large number of fins. The entropy generation number (4.10) can be expressed as a function of Re_D and γ. Representative results of the numerical work of minimizing N_S are shown in Fig. 4.3. The entropy generation number N_S has a clear minimum with respect to the pin diameter Re_D, when γ, B, and M are fixed.* The optimum pin diameter $Re_{D,opt}$ increases if the slenderness ratio decreases. This general trend is summarized in the right half of Fig. 4.3, for the range $5 \leq \gamma \leq 15$, $10^{-8} \leq B \leq 10^{-5}$. When the slenderness ratio is fixed, the optimum pin diameter decreases as the fluid friction becomes more important in the entropy generation total (i.e., as B increases).

Another practical design constraint worthy of consideration is the fin volume. This constraint is forced upon the designer by the high cost of construction materials such as copper. A dimensionless group which is proportional to the volume of the pin fin is $V = Re_D^{2}\, Re_L$. The entropy generation number

---

* $M = (k/\lambda)^{1/2}/Pr^{1/6}$.

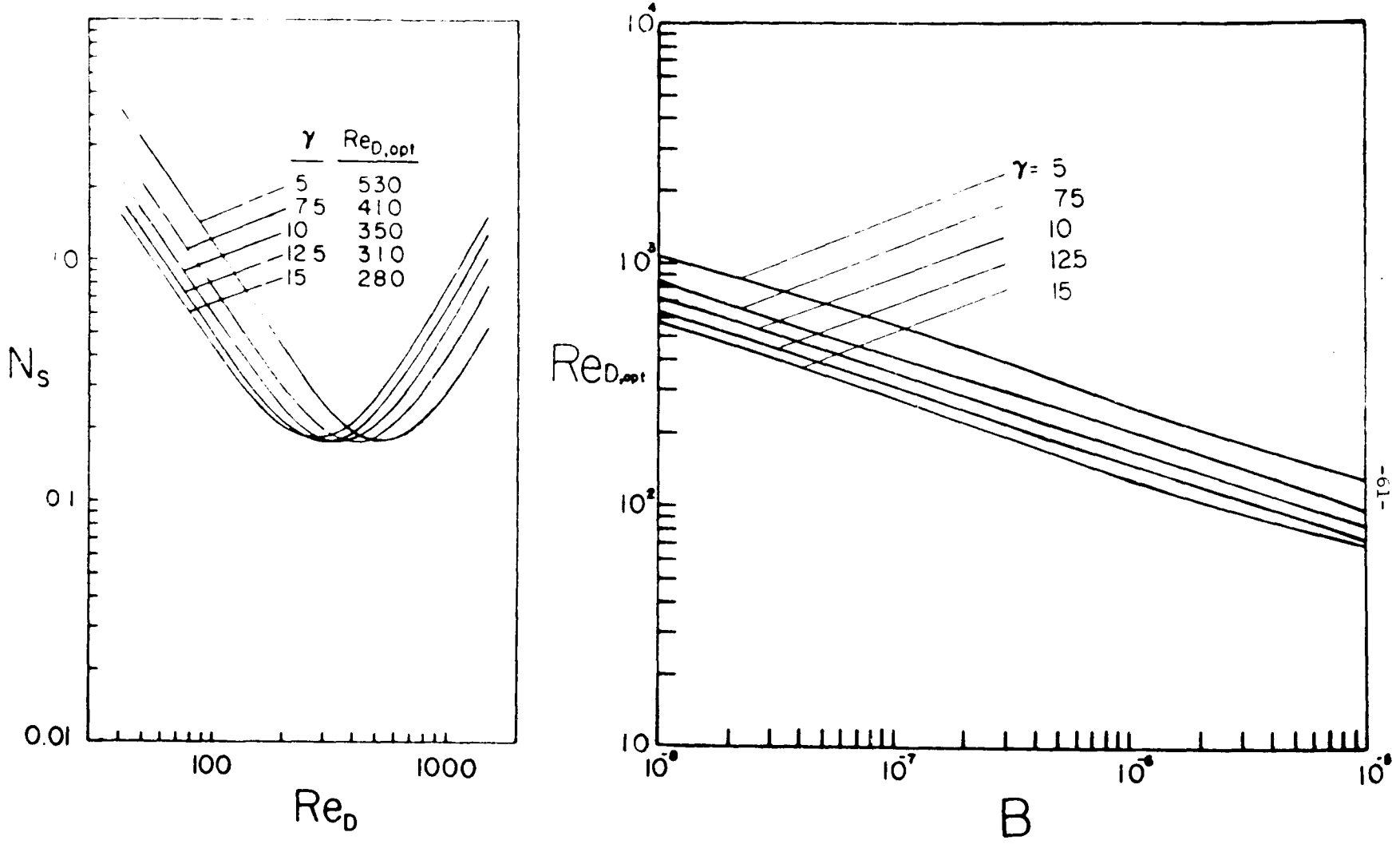

Fig. 4.3. Pin fin optimization. Left side: entropy generation number vs. pin diameter ($B = 10^{-7}$, $M = 100$). Right side: optimum pin diameter vs. friction irreversibility parameter B ($M = 100$).

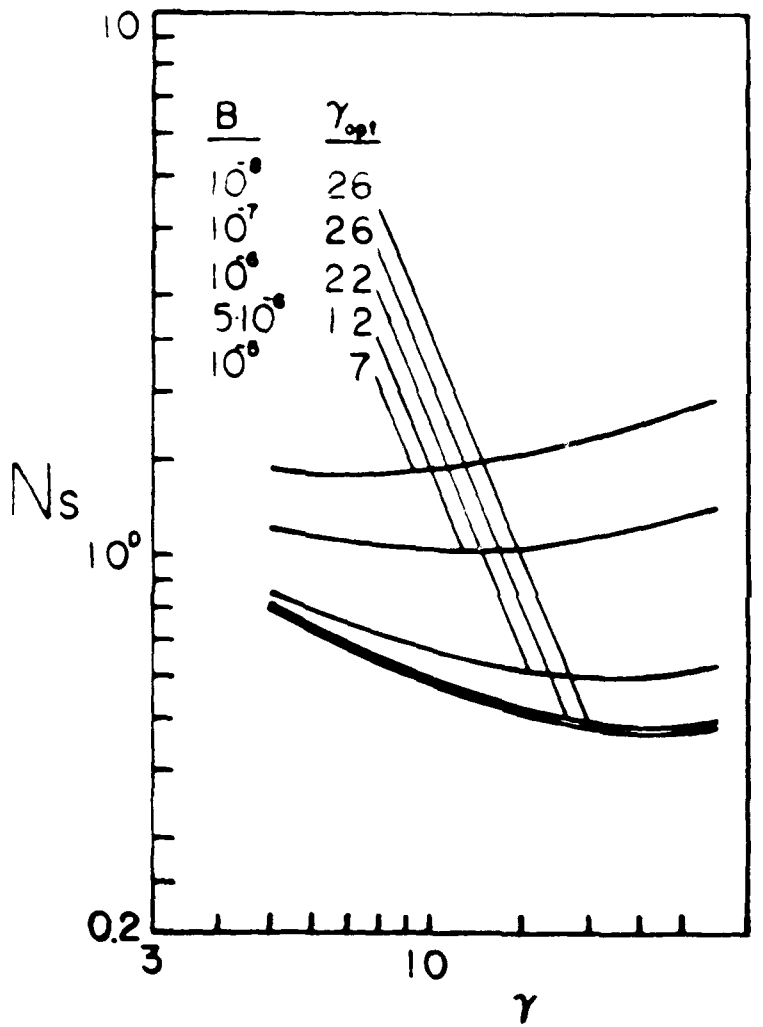

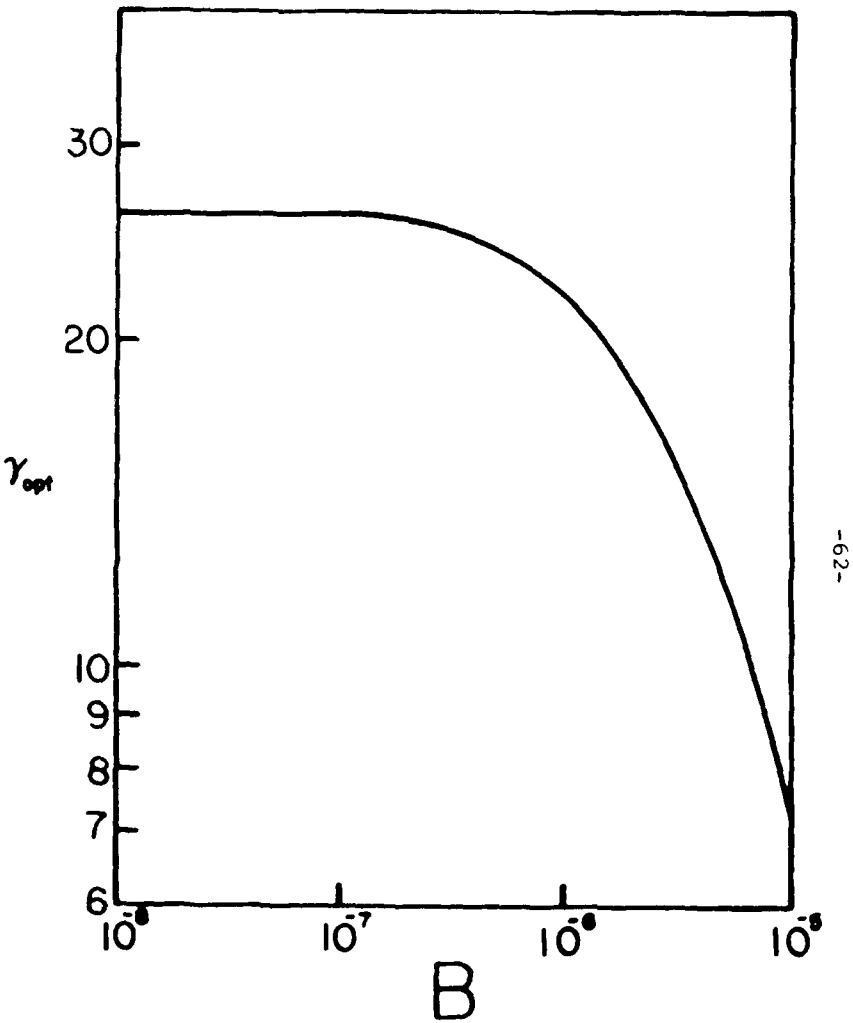

Fig. 4.4. Pin fin optimization subject to volume constraint ($V = 10^7$, $M = 100$). Left side: entropy generation number vs. slenderness ratio. Right side: optimum aspect ratio vs. friction irreversibility parameter B.

(N_S) can be expressed in terms of V and another geometric variable, for example, the slenderness ratio. On the left side of Fig. 4.4 we show the general behavior of the entropy generation number N_S, as γ and B vary subject to the constant volume constraint. The optimum slenderness ratio γ_{opt} for minimum N_S is summarized in the right half of Fig. 4.4: above a certain value of friction parameter B the optimum ratio γ_{opt} drops off rapidly as B increases.

4.3 Plate Fins

In this section we focus on fin geometries which can be modeled as thin conducting plates parallel to the flow direction. Fins of this type vary widely with respect to the shape and cross-section of the surface swept by the flow: in many cases the fin is wide at the base and narrow at the tip, in approximate agreement with Schmidt's principle of material reduction in a fin with fixed heat transfer [4.5]. Below, we consider the minimum entropy generation design of three frequently used plate fin geometries, illustrated in Figs. 4.2(b), (c), and (d).

Rectangular Plate Fin. The simplest plate fin geometry is shown schematically in Fig. 2(b). The minimum irreversibility design of this fin requires the selection of three geometric parameters, the length L, the breadth (length swept by fluid) b, and the plate thickness δ, where $L >> b >> \delta$. As in the preceding section, we are placing the study in the limit where the plate fin is slender ($b << L$); in this limit we rely on laminar heat transfer and skin friction results for two-dimensional flat plates [4.4]:

$$\bar{h} = 0.664 \frac{k}{b} Re_b^{\frac{1}{2}} Pr^{1/3}, \quad C_f = \frac{F_D}{\rho U_\infty^2 bL} = 1.328 Re_b^{-\frac{1}{2}} \tag{4.14}$$

The entropy generation number for a rectangular plate fin in laminar flow becomes

$$N_S = (S_{gen})_{fin} \Big/ \frac{q_B^2 U_\infty}{k \nu T_\infty^2}$$

$$+ \frac{(k/\lambda)^{1/2}}{1.15 \, Re_\delta^{1/2} \, Re_b^{3/4} \, Pr^{1/6} \tanh(mL)} + 1.328 \, B \, Re_L \, Re_b^{1/2} \qquad (4.15)$$

where

$$B = \rho \nu^3 k T_\infty / q_B^2 , \quad mL = 1.15 \left(\frac{\lambda}{k}\right)^{1/2} Pr^{1/6} \, Re_L \, Re_b^{-1/4} \, Re_\delta^{-1/2} \qquad (4.16)$$

From the outset we note that the plate thickness δ appears only in the heat transfer term of N_S, consequently, Re_δ does not play a trade-off role in the minimization of N_S. Since in most practical applications δ is determined by considerations such as price, availability and machinability of sheet metal, it makes engineering sense to regard Re_δ as fixed. The minimization of N_S with respect to Re_b and Re_L is achieved by solving the simultaneous set of equations $\partial N_S / \partial Re_b = 0$ and $\partial N_S / \partial Re_L = 0$: the optimum geometry for minimum entropy generation is explicitly given by

$$Re_{b,opt} = 0.984 \, B^{-2/3} \, Re_\delta^{-2/3} , \quad Re_{L,opt} = 0.685 \, (k/\lambda)^{1/2} \, Re_\delta^{1/3} \, Pr^{-1/6} B^{-1/6} \qquad (4.17)$$

This also means that the optimum slenderness ratio $\gamma = L/b$ is

$$\gamma_{opt} = Re_{L_{opt}} / Re_{b_{opt}} = 0.696 \, M \, B^{1/2} \, Re_\delta \qquad (4.18)$$

In conclusion, the optimum plate fin dimensions b and L can be

calculated directly using equations (4.17) as soon as the base heat flux (q_B), the flow field and the sheet metal thickness (δ) are known. It is necessary to keep in mind that the present formulas are valid only in the laminar regime, $Re_{b_{opt}} < 5 \times 10^5$, and in the "slender shape" limit $\gamma_{opt} >> 1$. Similar results can be developed numerically for the turbulent regime, by replacing equations (4.14) with appropriate correlations for turbulent heat transfer and skin friction.

If the thermodynamic optimization of the plate fin is subjected to the constraint of fixed material (volume) $V = Re_L\, Re_b\, Re_\delta$, the entropy generation number becomes

$$N_S = \frac{M\,\gamma^{\frac{1}{2}}}{1.15\,V^{\frac{1}{2}}\tanh(mL)} + 1.328\,B\,\frac{V^{\frac{1}{2}}\,\gamma^{\frac{1}{2}}}{\eta^{\frac{1}{2}}} \qquad (4.19)$$

where $\gamma = Re_L/Re_b$, $\eta = Re_\delta/Re_b$ and $mL = 1.15\,V^{1/12}\,\gamma^{4/3}/(M\,\eta^{1/6})$. Figure 4.5 shows the trade-off roll played by the geometric aspect ratio $\gamma = L/b$. The optimum aspect ratio γ_{opt} for minimum irreversibility can be determined numerically based on calculations of the type illustrated in the left half of Fig. 4.5. The general behavior of the γ_{opt} result is shown in the right half of the figure, for fixed V, M and η. The optimum aspect ratio γ_{opt} reaches a plateau below a certain value of friction parameter B; as B increases above $\approx 10^{-6}$, the optimum aspect ratio γ_{opt} decreases rapidly.

Rectangular plate fin of trapezoidal profile. A relatively more complex plate fin geometry is represented in Fig. 4.2(c). This time the fin longitudinal section is trapezoidal, again in the spirit of E. Schmidt's principle of material (volume) minimization [4.5]. This geometry has another important advantage over the rectangular shape of Fig. 4.2(b): the tapered profile makes trapezoidal

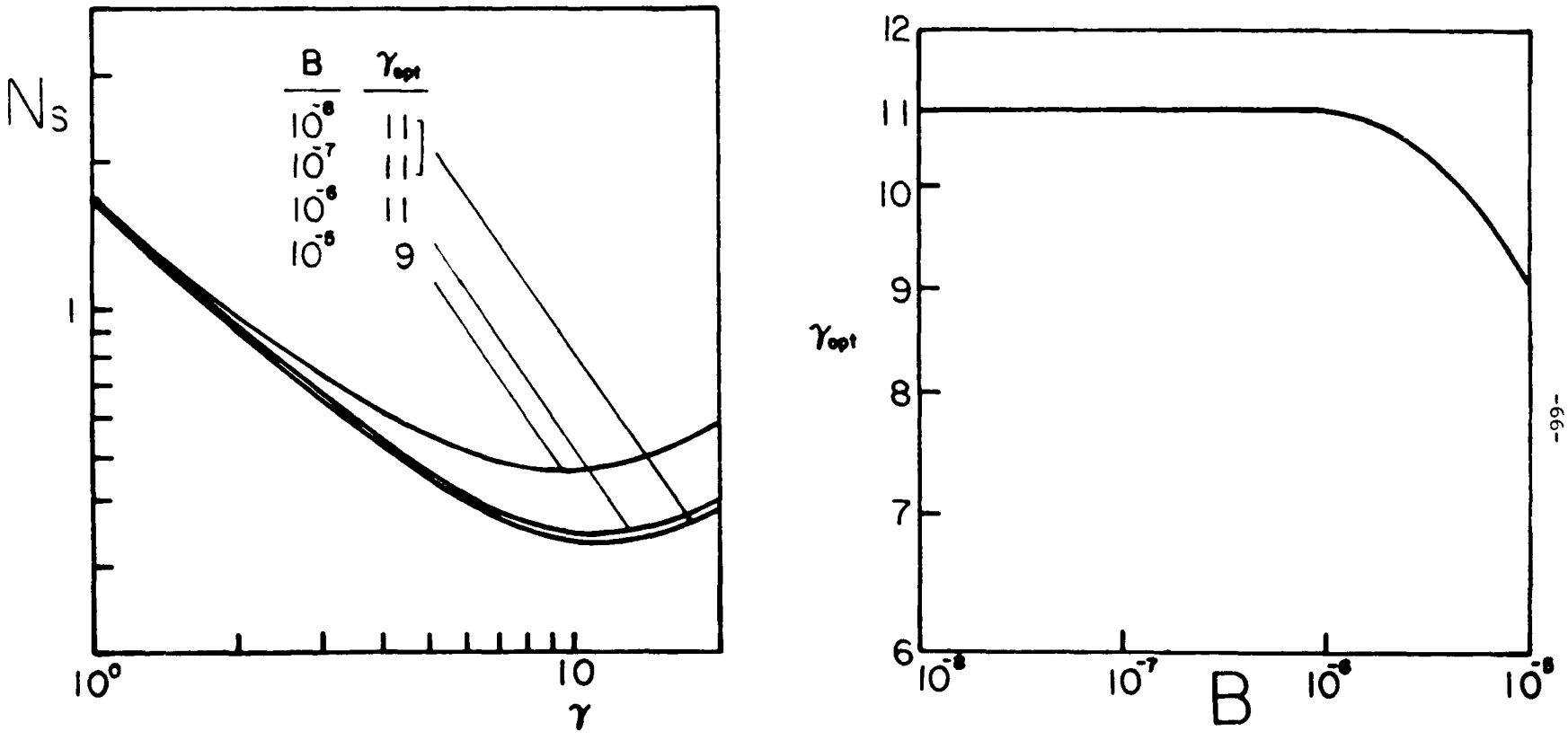

Fig. 4.5. Plate fin optimization ($V = 10^6$, $M = 100$, $\eta = 0.1$). Left side: entropy generation number vs. plate aspect ratio. Right side: optimum plate aspect ratio vs. friction irreversibility parameter B.

fins accessible to metal-cutting operations designed to remove the fin-to-fin material. The minimum entropy generation design of this class of fins can be approached along the same lines as the design of rectangular fins.

In the interest of brevity, we illustrate only a set of results abstracted from [4.1]. The entropy generation rate depends on four geometric parameters Re_L, Re_b, Re_{δ_e}, and α. Whether or not all four parameters may be considered independent depends on specific circumstances, particularly on the constraints faced by the designer (fixed cost, volume, base area, etc.). In Fig. 4.6, we show numerical results obtained in the case when b, δ_e, and α are fixed by design: the only geometric variable in this case is the fin length L (dimension perpendicular to the wall). Choosing the optimum Re_L for minimum entropy generation is geometrically equivalent to choosing the optimum base thickness Re_{δ_B} since $Re_{\delta_B} = Re_{\delta_e} + 2\, Re_L \tan\alpha$. The left side of Fig. 4.6 shows that N_S has a sharp minimum with respect to Re_{δ_B}. The optimum values of base thickness Reynolds number are reported in the right half of Fig. 4.6 for the case $Re_{\delta_e} = 100$ in the range $5^\circ \leq \alpha \leq 10^\circ$. We find that the optimum fin size (Re_{δ_B}) decreases as the fluid friction effect (B) becomes more pronounced, in agreement with conclusions reached in previous examples. Further, we see that in the α range considered, the angle α has a relatively minor impact on the optimum fin size for minimum irreversibility.

Triangular plate fin of rectangular profile. To the thermodynamic designer, this geometry is challenging due to the absence of convenient correlations for heat transfer and fluid friction in the three-dimensional boundary layer flow which, in most certainty, will cover the triangular faces of the fin. This analytical difficulty can be partially dealt with in the limit $D << L$, where the three-dimensional effects will be minor. In this limit, we can approximately treat the sharp-pointed triangular plate as a flat plate in parallel flow, with

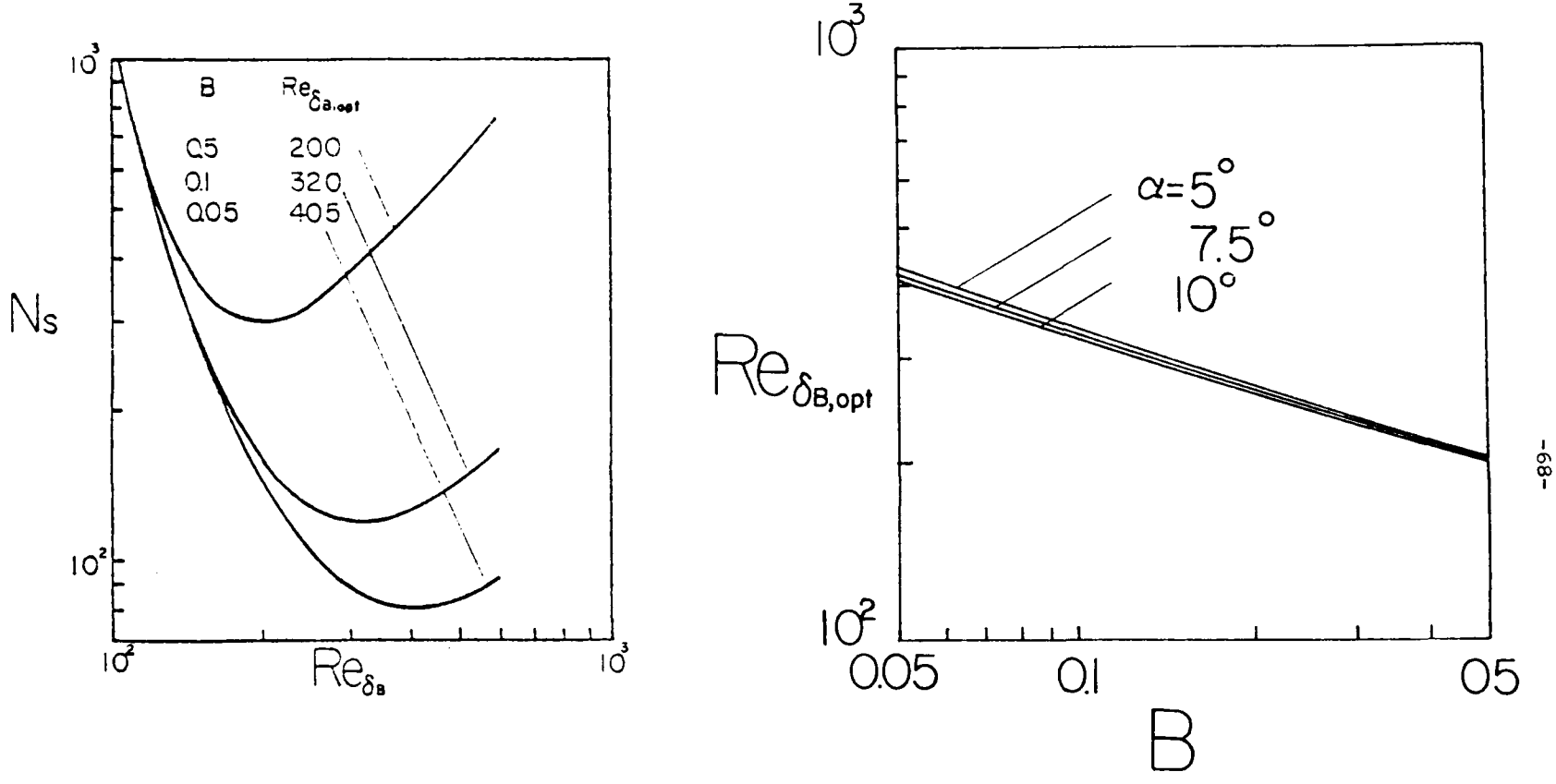

Fig. 4.6. Thermodynamic optimization of plate fins of trapezoidal profile ($\alpha = 10°$, $Re_{\delta_e} = 100$). Left side: entropy generation number vs. geometric aspect ratio. Right side: optimum aspect ratio vs. friction irreversibility parameter B.

the special property that the length swept by the flow (y) is a function of longitudinal position (x). It is worth pointing out that the $D << L$ limit is in full agreement with the uni-directional heat conduction model adopted in section 4.1.

The analytical path leading to the entropy generation rate formula is similar to the method used in the earlier examples [4.1]. Again, in the interest of brevity, we report only a number of representative results.

The entropy generation rate depends on three geometric parameters, Re_D, Re_L and Re_δ. In Fig. 4.7, we report a sample of optimum fin size results for cases where the triangle aspect ratio $a = Re_L/Re_D$ is fixed. The fin irreversibility N_S reaches a clear minimum at a specific value of fin base width, Re_D; the optimum fin size Re_D depends on the relative importance of fluid friction irreversibility (B), on the metal-fluid combination (M), and on the plate thickness (Re_δ). The right hand side of Fig. 4.7 is a summary of minimum N_S results obtained for a number of common metal-fluid combinations involving copper, aluminum, water and air. Regardless of combination, the optimum fin size ($Re_{D,opt}$) decreases as the triangular shape of the fin becomes, by design, more slender.

4.4 Optimum Fin Matrix for Minimum Entropy Generation

The focus of the preceding sections was on individual fins. Thus, we developed concrete means for selecting the geometric parameters which allow the fin to perform its prescribed heat transfer job with minimum entropy generation. An equally important design approach consists of focusing on an assembly of fins and finding out which particular association (matrix, relative positioning) allows the assembly to perform its prescribed heat transfer job with minimum irreversibility. We illustrate this approach in this section. From the outset,

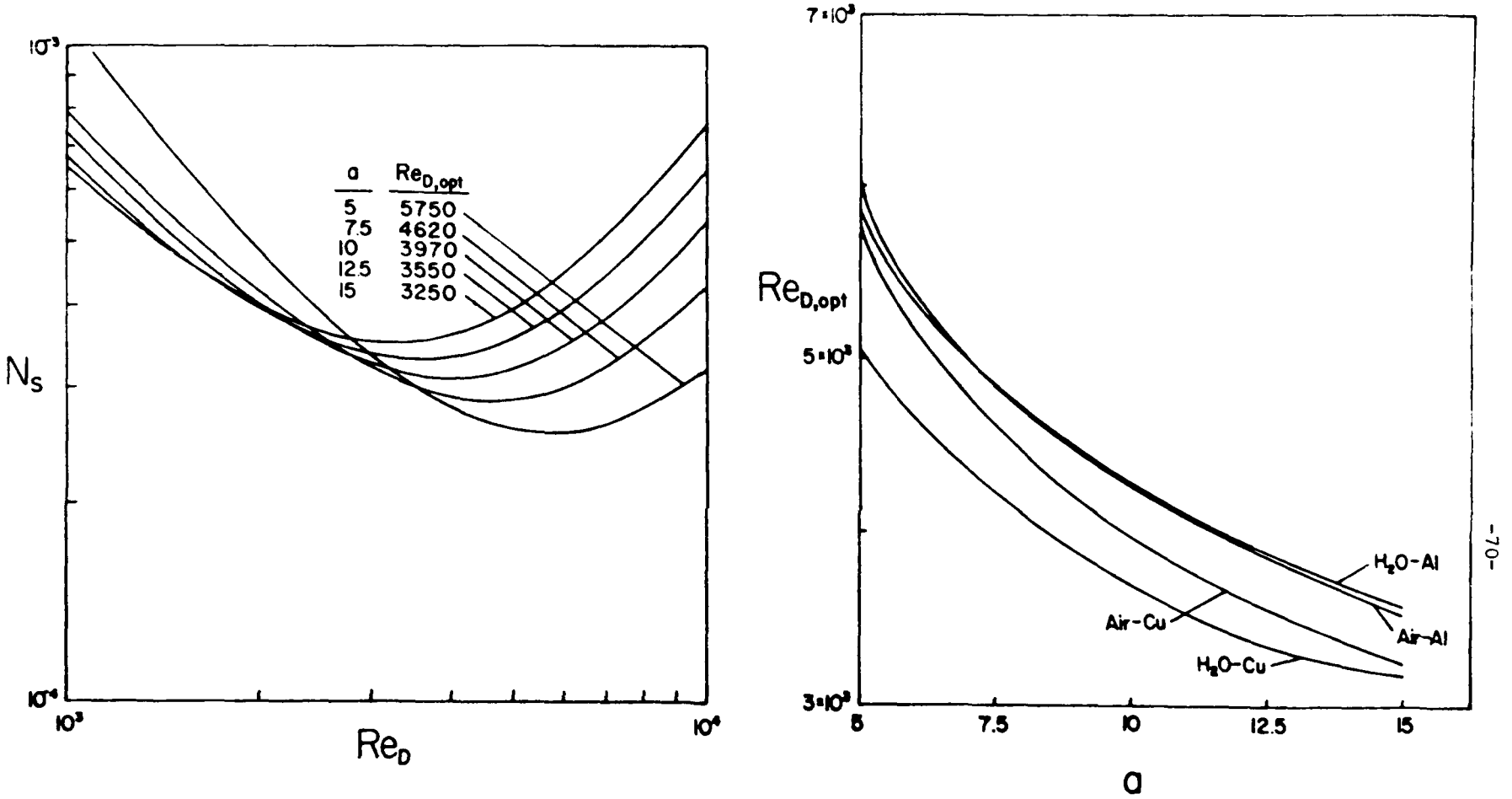

Fig. 4.7. Thermodynamic optimization of triangular plate fins (Air-Cu, Re_δ = 100). Left side: entropy generation number vs. base width. Right side: optimum base width vs. geometric aspect ratio a = L/D .

we note that the task of determining the optimum thermodynamic association of fins is made difficult by the lack of specific heat transfer and friction data on fin matrices.

The optimum association of pin fins can be determined concretely in the "isothermal fin" limit: in this limit the fin matrix is well-approximated by a tube bank in crossflow, for which Kays and London [4.6] report extensive heat transfer and fluid friction data. Consider a two-dimensional array of staggered fins. The overall dimensions, H and L, and the total heat transferred by the fin association, Q, are considered fixed by design. The total rate of entropy generation in the arrangement is

$$S_{gen} = \theta_S Q/T_\infty^2 + N F_D U_\infty/T_\infty \tag{4.20}$$

where

$$\theta_S = \frac{Q}{N \pi D W \bar{h}}, \quad F_D = \frac{1}{2}\rho U_\infty^2 C_D D W \tag{4.21}$$

Parameter N is the total number of fins populating the HxL area. For heat transfer and drag coefficients we have [4.6]

$$h = C_h \rho U_\infty c_p Pr^{-2/3} Re_D^{-0.4}, \quad C_D = C_f Re_D^{-0.18}, \tag{4.22}$$

where parameters C_f and C_h are available graphically as functions of transversal and longitudinal pitch, X_t and X_ℓ.

The entropy generation number N_S emerges as a function of the matrix (X_ℓ, X_t) and the diameter of each fin (Re_D). The left side of Fig. 4.8 shows the dependence of N_S on Re_D in one situation where the matrix is fixed. Clearly, there is an optimum Re_D which minimizes the total entropy generation rate; corresponding to this optimum diameter, there is an optimum number of

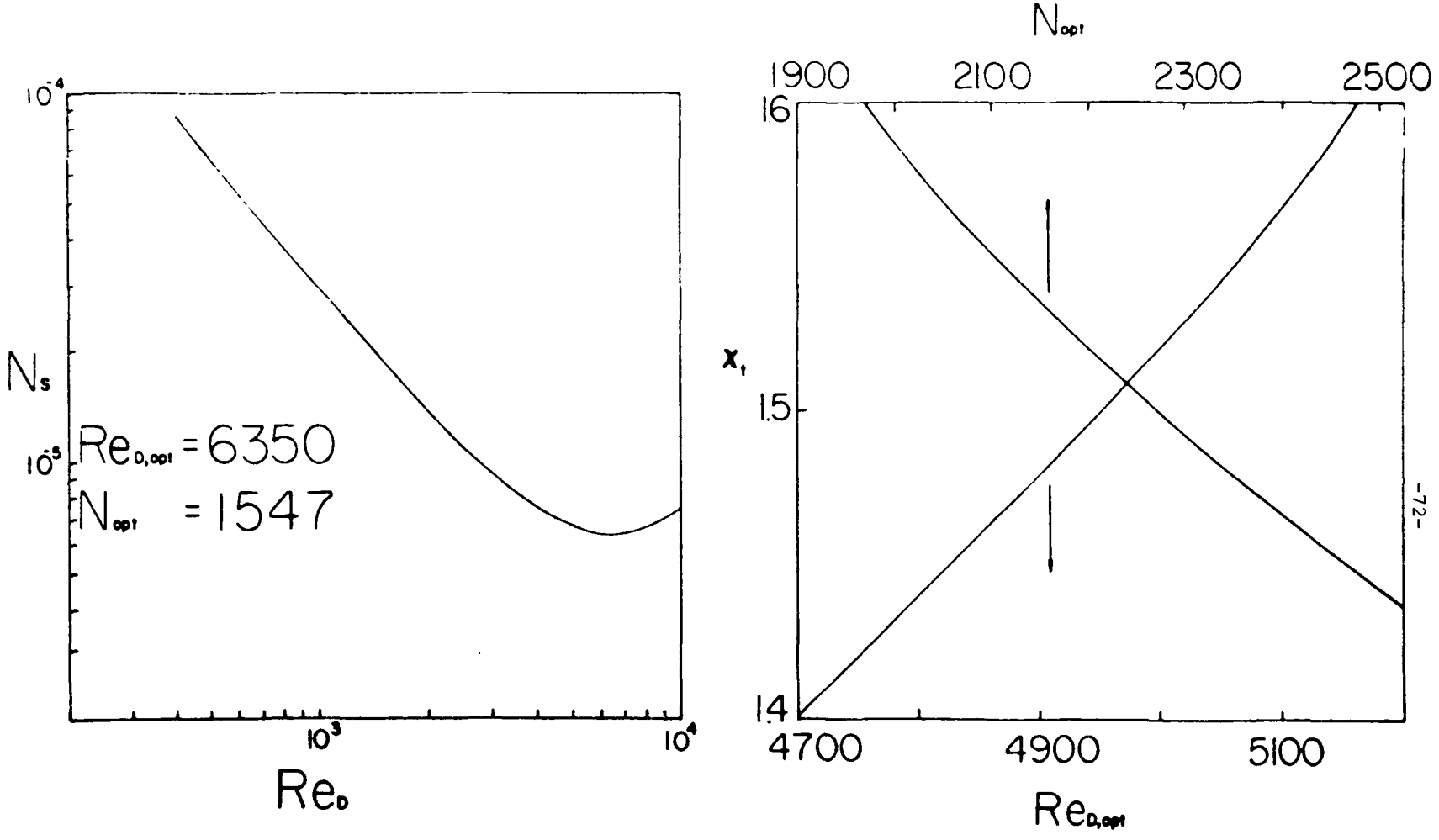

Fig. 4.8. Thermodynamic optimization of a pin fin array. Left side: entropy generation number vs. fin diameter ($X_\ell = 1$, $X_t = 1.7$, $B = 10^{-11}$). Right side: optimum fin diameter vs. fluid irreversibility parameter B ($X_\ell = 1.25$).

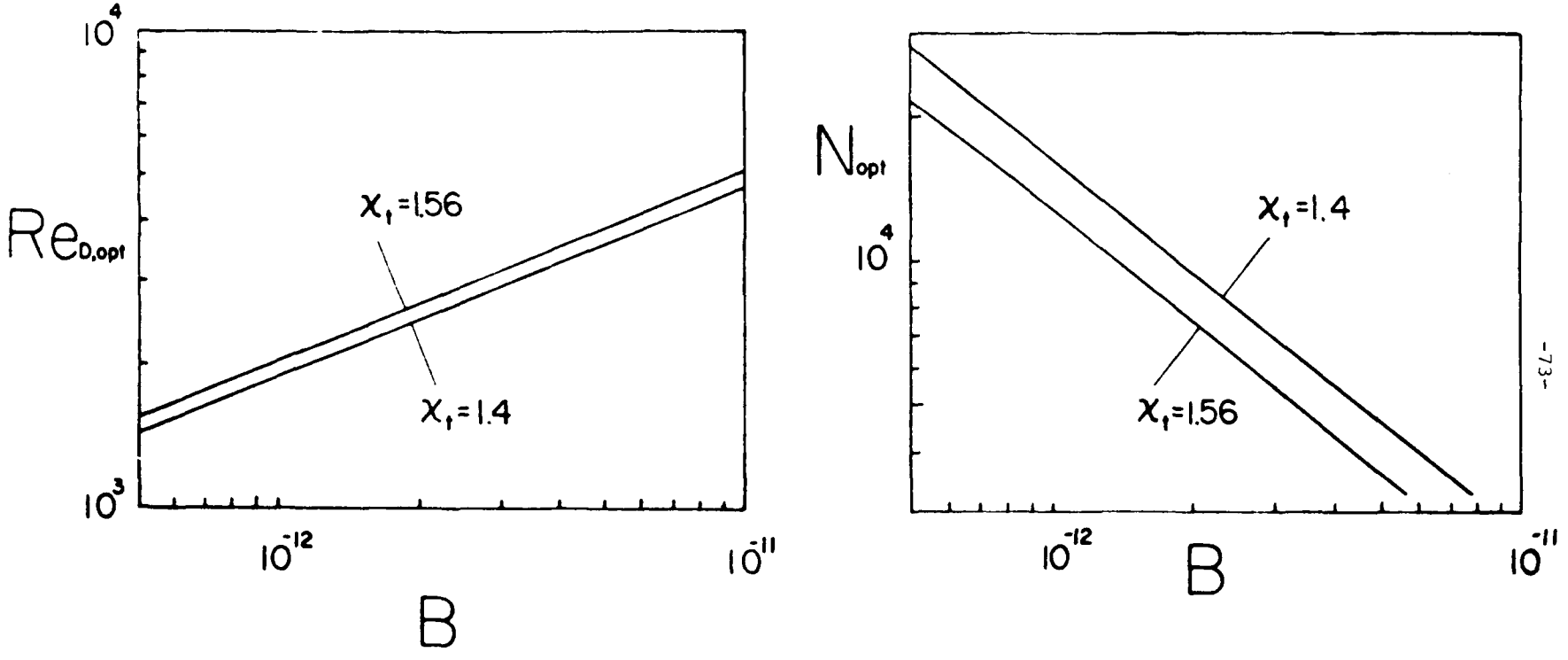

Fig. 4.9. The effect of friction irreversibility (B) on the optimum two-dimensional pin fin array. Left side: the optimum pin fin diameter. Right side: the optimum number of fins.

fins N to be planted on the surface under consideration. The right side of Fig. 4.8 summarizes the results of the N_S minimization procedure, for the case where only the longitudinal pitch X_ℓ is held constant. The optimum fin diameter increases with the increasing transversal pitch X_t, while the corresponding number of fins decreases.

The impact of varying the friction parameter B is illustrated in Fig. 4.9. If the matrix (X_ℓ, X_t) is held fixed, the optimum fin diameter increases as the friction effect becomes more proncunced. At the same time, the total number of fins (N) corresponding to $Re_{D,opt}$ decreases.

References

4.1 Poulikakos, D., "Fin Geometry for Minimum Entropy Generation," M.S. Thesis, Department of Mechanical Engineering, University of Colorado, Boulder, December 1980.

4.2 Kern, D.Q. and Kraus, A.D., Extended Surface Heat Transfer, McGraw-Hill, New York, 1972.

4.3 Bejan, A., Int. Journal of Heat and Mass Transfer, Vol. 21, p. 655, 1978.

4.4 Gebhart, B., Heat Transfer, McGraw-Hill, New York, 1971.

4.5 Schmidt, E., Zeit. d. ver Deutch Ing., Vol. 20, 1926, p. 885 and p. 947.

4.6 Kays, W.M., London, A.L., Compact Heat Exchangers, 2nd Edition, McGraw-Hill, New York, 1964.

Nomenclature

A	cross-sectional area
B	fluid friction irreversibility parameter
C_D	drag coefficient
C_F	skin friction coefficient
F_D	drag force
H	enthalpy
h	heat transfer coefficient
k	thermal conductivity of fin material
$\dot{m}$	mass flowrate
N	total number of isothermal pin fins (tubes)
N_S	entropy generation number
P	pressure
Pr	Prandtl number
Q	total heat transferred by the fin association
q''	local heat flux per unit area
q_B	heat flux through the fin base
S	entropy
S_{gen}	entropy generation rate
T	temperature
U	velocity
θ_B	temperature excess at the fin base, $T_B - T_\infty$
λ	thermal conductivity of fluid
μ	dynamic viscosity
ν	kinematic viscosity
ρ	density

5. CONCLUSIONS

This final report summarized the main results and conclusions of a two-year study of the thermodynamic implications of heat transfer augmentation [1.6-1.12]. In section 2 we reviewed a number of central topics in convective heat transfer, from the point of view of heat transfer as an entropy-producing mechanism. We saw the close relationship which exists between the irreversibility due to heat transfer and the irreversibility due to fluid friction in a given convective heat transfer configuration. In section 2 we developed a number of analytical tools designed to facilitate the numerical calculation of thermodynamic irreversibility in actual applications.

In section 3 we analyzed quantitatively the thermodynamic impact of using a proposed heat transfer augmentation technique. We showed that a technique's potential for reducing the rate of entropy generation depends strongly on the operating conditions of the heat exchanger passage in question. Specifically, the augmentation entropy generation number depends on the operating Reynolds number Re and on the irreversibility distribution ratio ϕ (the ratio of fluid friction irreversibility divided by the irreversibility associated with imperfect thermal contact). When the operating conditions of a certain component are specified (Re,ϕ), it is possible to assess the relative thermodynamic merit of various heat transfer augmentation techniques proposed for the same application. This comparison is done on the basis of plots N_S (Re,ϕ) as shown in Figs. 3.2-3.14; each of these plots is the property of a well-defined heat transfer augmentation technique.

Finally, in section 4 we considered the entropy generation associated with the use of extended surfaces (fins) in cross-flow. We showed that the sizing

(thermodynamic selection) of an individual fin always involves a trade-off between heat transfer and fluid friction irreversibilities. In the cases outlined in this report, the thermodynamic optimization of individual fins could be carried out based on fairly simple analysis. In general, as demonstrated in a more detailed report [1.12], the thermodynamic selection of finned surfaces can be pursued numerically. The main conclusion of this last phase of our study is that it is possible and, indeed, advantageous to conceptualize finned surfaces which perform their prescribed heat transfer duties and, at the same time, generate the least amount of entropy in the engineering system in which they function.

Overall, our study illustrates the importance of the Second Law of Thermodynamics in the development of efficient power systems. Our study shows how to evaluate the change in thermodynamic irreversibility (entropy generation) associated with a proposed design change, and how to make the right exergy-saving decisions. Although this final report is only a partial review of the work made available through individual publications [1.6-1.12], it is hoped it can alone serve as starting point for future Second Law analyses of power systems.


DATE
ILME